ANALYSIS OF DEFORMATIONS AND INSTABILITY IN EXPLOSIVE FORMING

By

S. C. BAJPAI

DEPARTMENT OF MECHANICAL ENGINEERING
INDIAN INSTITUTE OF TECHNOLOGY, KANPUR
DECEMBER, 1979

ANALYSIS OF DEFORMATIONS AND INSTABILITY IN EXPLOSIVE FORMING

A Thesis Submitted
In Partial Fulfilment of the Requirements
for the Degree of
MASTER OF TECHNOLOGY

By

S. C. BAJPAI

to the
DEPARTMENT OF MECHANICAL ENGINEERING
INDIAN INSTITUTE OF TECHNOLOGY, KANPUR
DECEMBER, 1979

dedicated to my

PARENTS

who missed me

On-many occassions, on-many happy moments

CERTIFICATE

This is to certify that the work entitled "An Analysis of Deformations and Instability in Explosive-Forming" has been carried out under my supervision and has not been submitted elsewhere for a degree.

24/12/79

December 1979

G.S. KAINTH
ASSISTANT PROFESSOR
DEPARTMENT OF MECHANICAL ENGINEERING
INDIAN INSTITUTE OF TECHNOLOGY, KANPUR

ACKNOWLEDGEMENT

The author wishes to express his profound gratitudes to his thesis supervisor Dr. G.S. Kainth for valuable advice, encouragement and helpful criticisms throughout the course of this work.

He sincerely acknowledges the encouragement and helpful suggestions rendered by Shri R.C. Gupta.

The author highly appreciates the help provided by his friends Subodh, A.K. Chaturvedi, R.P. Yadav and U.C. Ray.

He gratefully acknowledges the assistance rendered by M/s. Rahman, Joginder Singh, O.P. Bajaj, V.N. Bajpai, R.M. Jha and the supporting staff of the Mechanical Engineering Department.

The author expresses his appreciation to Shri S.N. pandey for the flawless typing of the manuscript, to Shri B.B. Srivastava for preparing excellent drawings and to Shri R.S. Dwivedi for excellent duplicating work.

December 23, 1979

S.C. BAJPAI

TABLE OF CONTENTS

PAGE

PAGE

LIST OF FIGURES

ABSTRACT

A theoretical analysis of explosive forming based on the theory of hydrostatic bulging of a circular diaphragm clamped at the periphery is made. Dynamic effects due to the energy pulse generated by the underwater explosion of a charge and consequent strain-rate effects are incorporated in the analysis. The analysis is used for predicting explosive charge weight to produce a dome of given height of deformation. The theoretical predictions are compared with experimental values.

Limit strains are predicted for Aluminium-1100, 70-30 Brass and stainless steel - 304 sheets of different thicknesses taking into consideration the effect of initial sheet thickness, initial grain size and surface roughness. Theoretically predicted values of limit strains are compared with experimental results.

NOTATION

a	radius of diaphragm
A, B	constants of Swift's stress-strain relationship
A_1, c	constants of explosive
d_o	average grain diameter of unstretched sheet
f_i	thickness parameter at instability
g	gravitational constant
h	polar height of formed dome
k	empirical constant in relation $R = kd_o\bar{\epsilon} + R_o$
L_o, L	initial and current length of element in roughness model
m	strain-rate index
M	constant defining a surface roughness peak
n	strain hardening index
N	number of grains in length L
p	pressure generated by explosive at time t
p_d	dynamic effective pressure generated by explosive
p_h	hydrostatic pressure required for hydrostatic bulging
p_m	maximum value of pressure p
R_o, R	initial and current surface roughness of sheet metal

S_o stand-off distance

S distance of a point on diaphrgm from charge

t_d time of deformation of blank

T_o initial thickness of undeformed blank

T current thickness of deforming blank

V_a average velocity of deformation of blank

w specific weight of material of sheet

W weight of explosive charge

x principal stress-ratio

Y radial distance of a point from centre of diaphragm

α_1 constant for an explosive

ρ radius of curvature of formed dome

$\varepsilon_1, \varepsilon_2, \varepsilon_3$ hoop, radial and thickness strains

$\bar{\varepsilon}$ representative strain

$\bar{\varepsilon}_i$ representative instability strain

$\dot{\bar{\varepsilon}}$ representative strain-rate

ε^* representative limit strain

$\bar{\sigma}_p$ representative polar stress

$\sigma_1, \sigma_2, \sigma_3$ stresses in hoop, radial and thickness directions

SUBSCRIPTS

A uniformly stressed region

B grooved region

CHAPTER I

INTRODUCTION AND LITERATURE SURVEY

1.1 INTRODUCTION

Explosive forming is useful for formirg sheet materials specially for high strength materials such as Titanium and Stainless steel. One of the earliest applications of explosives to metalworking was that of Munroe (1888) who used explosives for engraving iron plates by imprinting a design on a block of explosive [1,2].

During Second World War extensive studies on underwater explosions were made for defence purposes. The results of these studies have been compiled by Cole [3] and Penny et al. [4].

Systems employed in explosive forming are broadly classified into (a) confined or closed system and (b) unconfined or open system. Closed system is suitable for shaping of small components. In unconfined system, explosion takes place generally in water medium such that only a part of the total energy is available for deformation process. Explosive forming is generally done by underwater stand-off operation in which case the charge is located some distance away from the sheet.

In order to estimate explosive charge, in an underwater stand-off operation, it is necessary to know the pressure, impulse and energy which exist at a distance from the energy source at a given time. Rinehart and Pearson [5] have presented the required information in the form of nomographs.

1.2 EFFECT OF VARIOUS PROCESS PARAMETERS

Various research workers [6 - 14] have conducted explosive forming experiments to show the effect of process parameters. The mode of deformation of a clamped circular blank during free forming was studied by Hudson [15]. and Johnson et al. [10].

Ezra [16, 17] showed that stand-off distance has a marked effect on the shape of freely formed parts. Johnson, Kormi and Travis [12] investigated the effect of hydrostatic head in explosive deep drawing of circular blanks using plug-cusion technique. Johnson et al [11] investigated the effect of shape of charge. The deformation obtained from a spherical charge was found to be slightly greater than that obtained by using a ring charge. Radial and thickness strains for the case of free forming are studied by Travis, Johnson [9] and Rekhi [18].

For estimating the explosive charge Ezra et al. [8, 19] developed a technique for relating the results of model testing for producing large components. The scaling law so developed is useful as a first approximation in predicting the charge weight. A simple analysis for predicting charge size for small parts is given by Noble and Oxley [20]. However, the accuracy of their prediction depends upon the selection of correct efficiency factor which varies from 0.4 to 1.0. [18]

1.3 MATERIAL PROPERTIES UNDER IMPULSIVE LOADING

Rinehart and Pearson [21] discussed the characteristics of impulsive loading. The loading in explosive forming process is an example of impulsive loading.

There is a pronounced effect of high pressures on mechanical properties specially under impulsive loading. The work of Bridgeman in this field is notable and a few of his results are summarised in references [22,23].

Many investigations [24-30] have been carried out to determine a relationship between stress and strain in a material which is loaded dynamically. These investigaters have recognised that a difference exists between the performance of materials under static and dynamic

conditions of loading. All the published data [24-38] lead to the conclusion that the yield strength and resistance to deformation increase with increase in strain-rate.

Several techniques are used to evaluate the effect of strain-rate on the properties of a material. Methods generally used are a) high speed tensile impact testing [24] b) firing of high velocity projectiles against targets [33] and c) explosive bulge testing [10]. In general, an increase in the rate of deformation increases a) yield strength of the material b) entire stress level of the flow curve and c) ultimate strength of the material.

Parker and Ferguson [34] performed a series of impact tests and showed that the dynamic yield strength is considerably greater than the static yield strength for various steels and aluminium alloys tested. Compbell and Duby [38] found that the compressive yield strength of mild steel increased upto 2.5 times the static value. Nadai and Manjoine [35] and Johnson et al. [36] reported that the effects of high speed on the deformation of aluminium and its alloys are similar to those on steels. A limited number of tensile tests carried out [25] on 60-40 and 70-30 brass at ambient temperature showed that

the yield point increased to 1.45 times the static value. The increase in strength is even more pronounced when dynamic testing is carried out at elevated temperatures. [35]. Sturgess and Bramley [37] used impact forming devices to find dynamic stress-strain relationship for mild steel. They established the double power constitutive equation $\sigma_{dynamic} = \sigma_{static} \dot{\varepsilon}^{m}$ where the strain-rate index m = 0.17 for mild steel.

1.4 INSTABILITY IN BIAXIAL TENSION

Instability of circular metalic diaphragm clamped at periphery and deformed by hydrostatic pressure is considered by Johnson and Mellor. [39] Marciniak and Kuczynski [40] assumed that at condition of instability an initial inhomogeneity, expressed by local thickness ratio, in the sheet material develops into a groove. They proposed a theory to work out a value of limit strain at which necking in the workpiece is initiated. Many experimental studies have been carried out to determine the forming limit diagrams for sheet materials [41-43].

Miyano [44] experimentally studied the effect of initial thickness of sheet material on limit strain for annealed Aluminium. He found that the fracture strains decreased with decrease in thickness of the specimen.

Minh et al. [45] showed that the forming limit increases with increase in blank thickness since the effect of an initial inhomogeneity or void of a given size assumes lesser significance as the sheet thickness increases.

Kienzle [46], Osakada and Oyane [47] and Fukuda et al. [48] have investigated the effect of surface roughness on limit strain. Yamaguchi and Mellor [49] presented a theoretical analysis to work out instability strain in isotropic sheet materials under biaxial tension taking into consideration the effect of initial sheet thickness, grain diameter and surface roughness. Parmar and Mellor [50] applied Marciniak-Kuczynski analysis at instability condition to find out limit strains in sheet materials for biaxial tension.

1.5 PRESENT WORK

In the present work hydrostatic bulging theory for a circular metalic diaphragm is modified for the case of explosive forming.

The basic problem in explosive forming is the estimation of explosive charge weight corresponding to a suitable stand-off distance to produce required shape consistent with the soundness of the product. However, a number of variables involved in the process such as dimensions of the blank, properties of the blank material,

shape of the component, type of explosive, stand-off distance and strain-rate need to be considered to predict charge weight. The present analysis takes into considerations the effect of all the above mentioned variables for estimating weight of explosive charge required for a given deformation.

The present analysis also includes the effect of initial sheet thickness, initial grain size and surface roughness for predicting limit strains for aluminium-1100, 70-30 brass and stainless steel-304.

CHAPTER II

THEORETICAL ANALYSIS FOR ESTIMATION OF EXPLOSIVE CHARGE WEIGHT

2.1 INTRODUCTION

The nature of pressure pulse generated by the underwater detonation of an explosive charge is used to estimate average pressure p_a. Hydrostatic pressure p_h, required for a given height of deformation of dome, is obtained by applying Johnson's [39] analysis for hydrostatic bulging. The hydrostatic bulging theory is modified by considering the effects of stand-off and strain-rate for the case of explosive forming. Finally, the weight of explosive charge required for a given height of deformation of dome is estimated by using the modified hydrostatic bulging theory.

2.2 EXPLOSIVE PRESSURE PULSE

When an explosive charge is detonated in water, a high intensity spherically expanding pressure pulse is initiated at the point of charge. The pressure reduces due to divergent nature of the wave front and energy losses in the medium. At any given distance from the centre of the charge, the idealised pulse has a pressure-time history as shown in Fig. 1. The pressure p at any

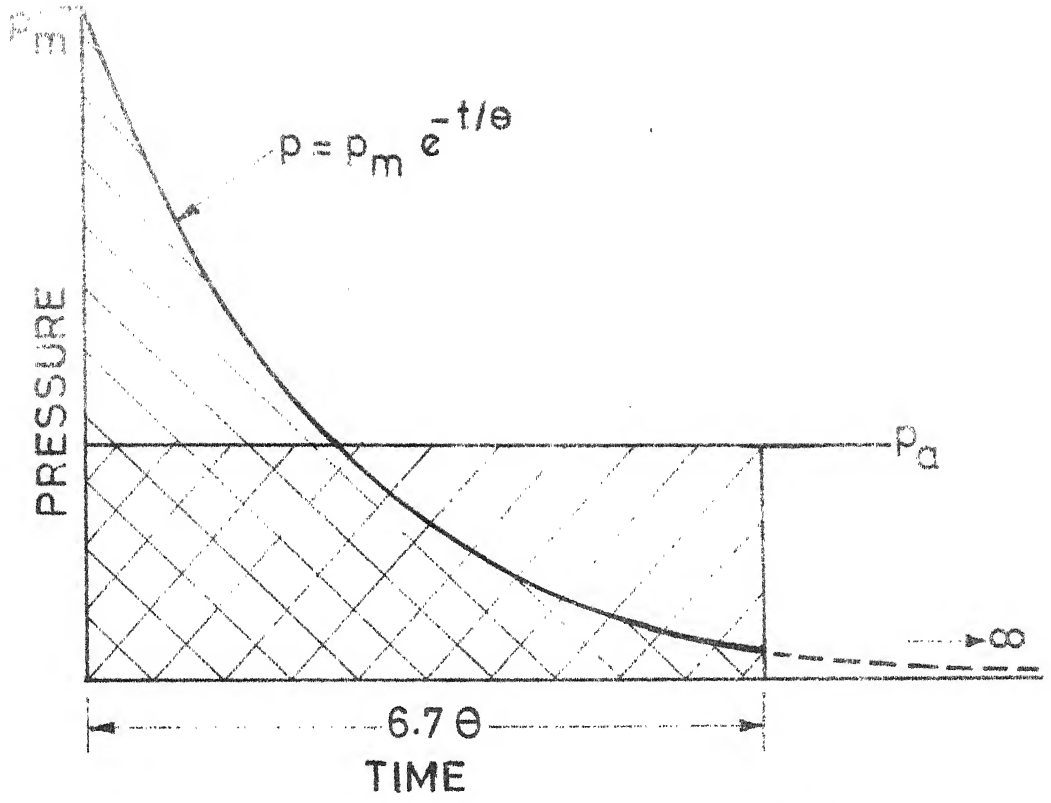

FIG.1 PRESSURE-TIME CURVE FOR UNDERWATER EXPLOSION

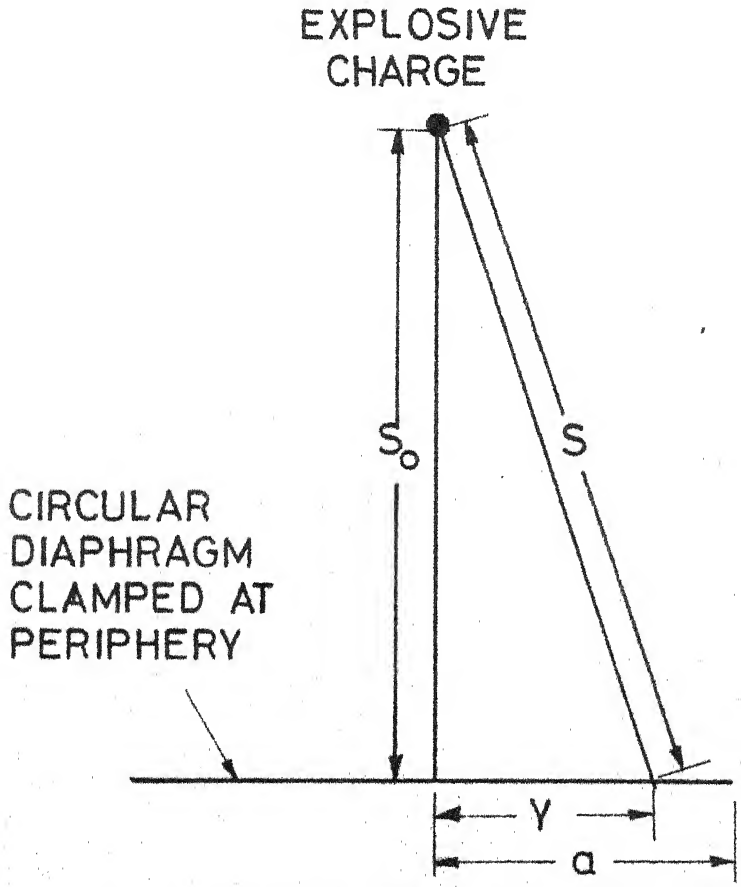

time t after the detonation is given by [51]

$$p = p_m e^{-t/\theta} \qquad (1)$$

where θ is the time constant which represents the time for the pressure to fall to a value 1/e times that of its peak value p_m. (e = 2.73) Rinehart [5] has given the following empirical relation to obtain the value of time constant θ,

$$\theta = 70 (W)^{1/3} \qquad (2)$$

where explosive charge weight W is in pounds and θ is in microseconds.

The distribution of maximum pressure along a plane, when a small spherical explosive charge is detonated at a stand-off distance S_o (Fig.2) is given by, [51]

$$p_m = 2A_1 \left[\frac{W^{1/3}}{S} \right]^{\alpha_1} \qquad (3)$$

The variations of peak pressure p_m along the radius of a diaphragm, for different cordtex explosive charges and for stand-off distances of 150 mm and 300 mm, are shown in Fig. 3. For the case of Cordtex explosive the constants A_1 and α_1 are taken to be 22500 and 1.13 respectively from reference [51]. It is seen from

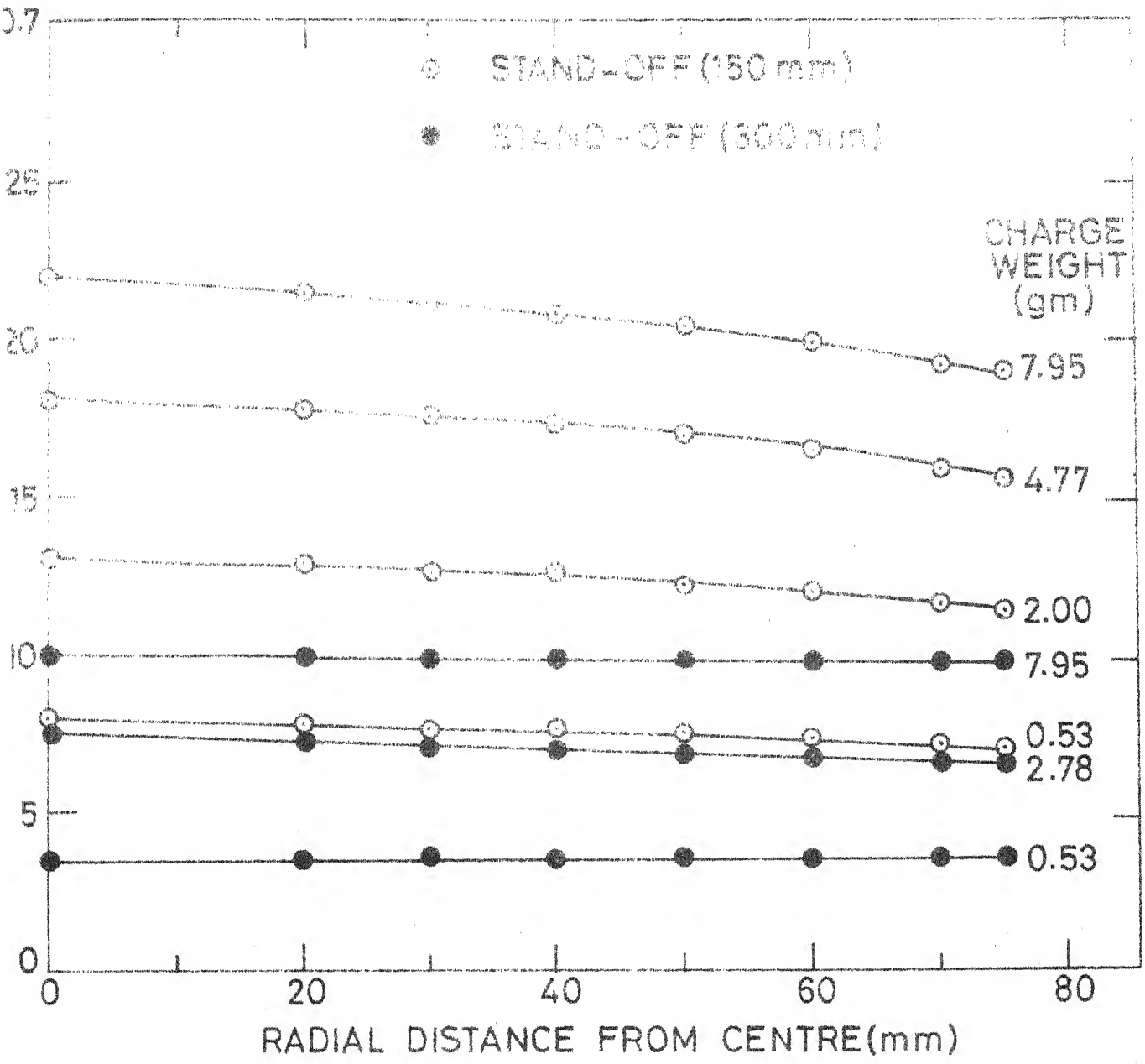

G.3 DISTRIBUTION OF MAXIMUM PRESSURE ALONG THE RADIUS OF THE DIAPHRAGM

Fig. 3 that the decrease of maximum pressure along the radius of the diaphragm becomes smaller as stand-off distance is increased. This reduction in pressure is 12 percent for 150 mm stand-off and 3.8 percent for 300 mm stand-off. Hence this small variation can be ignored in the analysis for obtaining average pressure.

The average pressure p_a is obtained by considering the area under p_m versus t curve (Fig.1)

$$\text{Area under the curve} = \int_o^t p_m \, e^{-t/\theta} \, dt \qquad (4)$$

The integration should, theoretically, be carried out over an infinite interval of time. However, in practice, this is not reasonable since the tail of the curve, being sustained at low level for a long time, will unduly reduce the average pressure p_a. A reasonable estimate is obtained if the integration is carried out over a finite interval of time. For explosives, the integration time is taken to be $t = c\theta$ where c is a constant depending upon the type of explosive. Thus, average pressure p_a is given by,

$$p_a = \frac{1}{c\theta} \int_{t=o}^{t=c\theta} p_m \, e^{-t/\theta} \, dt \qquad (5)$$

2.3 HYDROSTATIC BULGING OF A CIRCULAR DIAPHRAGM

If a circular sheet of metal is clamped at its periphery and subjected to hydrostatic pressure on one side, the shape of the deformed dome is approximately spherical specially in the region near the pole for the case of explosive forming [18].

The case of straining of sheet metal under equal biaxial tension [39] is used in the present analysis and the same is briefly outlined below. The stress in thickness direction σ_3 is either zero or negligible in comparison with other two stresses. Generally, elastic strains are neglected and Levy-Mises equations are assumed to apply. It is also assumed that principal axes do not rotate relative to the element being strained. Thus, for equal biaxial tension case $\sigma_1 = \sigma_2$ and $\sigma_3 = 0$.

For biaxial tension, Levy-Mises equations for principal directions are given by [39]

$$\frac{\varepsilon_1}{2-x} = \frac{\varepsilon_2}{2x-1} = -\frac{\varepsilon_3}{1+x} = \frac{\bar{\varepsilon}}{2(1-x+x^2)^{1/2}} \qquad (6)$$

For equal biaxial tension, stress-ratio $x=1$ and equation (6) may be written as

$$\frac{\varepsilon_1}{2} = \frac{\varepsilon_2}{2} = \varepsilon_3 = \bar{\varepsilon} \qquad (7)$$

Using the theory of hydrostatic bulging [32], the radius of curvature at the pole is given by the relationship (see Fig. 4)

$$h(2\rho - h) = a^2 \quad \text{or} \quad \rho = (h^2 + a^2)/2h \qquad (8)$$

The generalised strain $\bar{\varepsilon}$ is expressed in terms of height of deformation as

$$\bar{\varepsilon} = \varepsilon_3 = \ln (T_o / T) = 2\varepsilon_1 = 2\ln(1+h^2/a^2) \qquad (9)$$

Representative polar stress $\bar{\sigma}_p$ is given by

$$\bar{\sigma}_p = A (B + \bar{\varepsilon})^n \qquad (10)$$

Hydrostatic pressure p_h required for a given height of deformation is obtained as [39]

$$p_h = \frac{2 \bar{\sigma}_p \, T}{\rho} \qquad (11)$$

2.4 APPLICATION OF HYDROSTATIC BULGING THEORY TO EXPLOSIVE FORMING

The theory of hydrostatic bulging is modified to find out the explosive pressure and corresponding explosive charge required for a given height of deformation.

2.4.1 Effect of Stand-off

In the case of hydrostatic bulging the pressure acts radially on the surface of the diaphragm. Since the explosive charge is not placed at the centre of curvature of the deforming dome, the shock wave is not acting normal to the surface of the sheet but it is incident at an angle to normal to the sheet as shown in Fig. 4.

To evaluate the effect of angle of incidence of wave, consider an elemental width dr at a radius r on the deforming dome (Fig. 4). Normal force on elemental ring $dF_N = 2\pi r\, p_a \cos\psi\, dr$ where angle ψ is given by the geometry of the system as

$$\psi = \beta - \alpha = \frac{r}{\rho} - \frac{r}{R_o} = \left(\frac{1}{\rho} - \frac{1}{R_o}\right) r = k_1 r$$

Thus, total normal force F_N on the circular blank is given by

$$F_N = \int_{r=o}^{r=a} 2\pi r\, p_a \cos\psi\, dr$$

$$= \pi a^2 p_a \left[2 \left\{ \frac{\sin k_1 a}{k_1 a} - \left(\frac{1-\cos k_1 a}{k_1^2 a^2} \right) \right\}\right] \qquad (12)$$

or $F_N = \pi a^2 (p_a F)$ (13)

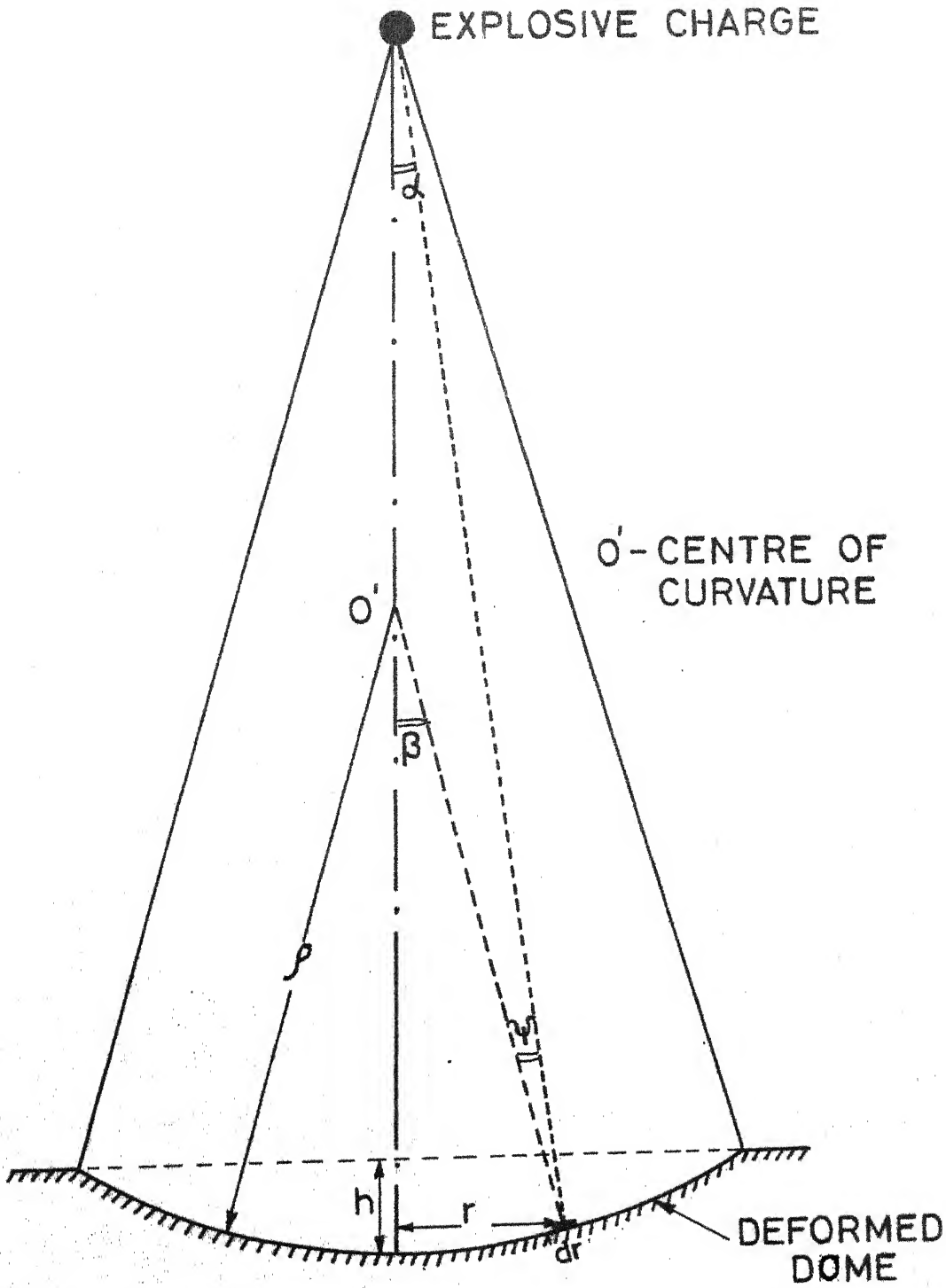

FIG. 4 EFFECT OF STAND-OFF ON INCIDENCE OF PRESSURE WAVE

where F is a factor which takes into account the effect of the position of charge on pressure exerted on the sheet such that the dynamic effective pressure p_d generated by the explosive is written as

$$p_d = F\, p_a \qquad (14)$$

The dynamic effective pressure p_d is assumed to act radially on the blank.

2.4.2 Strain-Rate Effect

In explosive forming processes, duration of the pressure wave is estimated to be considerably shorter than the time of deformation of the dome as shown below. A typical value of duration of pressure wave using equation (2) for 3.18 gms. of Cordtex explosive (c = 6.7) [51] is 90 microseconds. Whereas, the time of deformation to produce a dome of 38 mm height for Aluminium-1100 using 3.18 gms of Cordtex at 150 mm stand-off is estimated to be 720 microseconds as explained latter. Hence, the effect of the pressure generated by the shock wave due to detonation of explosive is essentially that of an impulse on all elements of the workpiece.

Rinehart [5] found that the dynamic yielding occurs at higher pressures than the pressure required for static yielding. Hence, dynamic pressure can be

related with hydrostatic pressure by,

$$p_d = K\, p_h \tag{15}$$

However, dynamic stress is given by Sturgess and Bramley [37] as,

$$\sigma_{dynamic} = A\, \bar{\varepsilon}^{n}\, \dot{\bar{\varepsilon}}^{m} = \sigma_{static}\, \dot{\bar{\varepsilon}}^{m} \tag{16}$$

Hence, considering equations (11), (15) and (16),

$$\frac{\sigma_{dynamic}}{\sigma_{static}} = \frac{p_d}{p_h} = \dot{\bar{\varepsilon}}^{m} = K \tag{17}$$

The factor K takes into account the strain-rate effects. The strain-rate is obtained by dividing the generalised strain at the pole by the time of deformation of the dome t_d. For the case of equal biaxial tension, the generalised strain $\bar{\varepsilon}$ is numerically equal to the thickness strain ε_3. Thus,

$$\dot{\bar{\varepsilon}} = \frac{\bar{\varepsilon}}{t_d} = \frac{\varepsilon_3}{t_d} \tag{18}$$

The time of deformation of blank t_d is found by considering the average velocity of deformation of blank V_a and maximum height of deformation. The average velocity of deformation is found by assuming linear variation of velocity from initial velocity V_o imparted

to the blank to final velocity which is zero.

2.4.3 Initial Velocity Imparted to the Blank

The initial velocity V_o imparted to the blank is obtained by equating the kinetic energy delivered by the explosive impulse to the plastic work done in deforming the dome.

Consider an infinitely narrow annulus of sheet of width dr of diaphragm as shown in Fig. 4. The volume of the annulus dV is given by

$$dV = 2\pi \; r \; dr \; T_o \qquad (19)$$

The work done δW on this infinitely narrow annulus of volume dV is given by

$$\delta W = \int \bar{\sigma} \; d\bar{\varepsilon} \; dV \qquad (20)$$

where $d\bar{\varepsilon}$ denotes the increament in representative strain of the element.

The following representative stress-representative strain relationship given by Swift for strain hardening material is used.

$$\bar{\sigma} = A \left(B + \bar{\varepsilon} \right)^n$$

Hence, the increamental work is given by,

$$\delta W = \int A \left(B + \bar{\varepsilon} \right)^n d\bar{\varepsilon} \; \delta V \qquad (21)$$

Integrating equation (21) for the entire blank, the total plastic work W required for deforming the blank is given by

$$W = \int_{r=0}^{r=a} 2\pi r A \frac{(B+\bar{\varepsilon})^{n+1}}{(n+1)} T_o \, dr \qquad (22)$$

For the case of equal biaxial tension, the representative strain $\bar{\varepsilon}$ is given by

$$\bar{\varepsilon} = \varepsilon_3 = 2\varepsilon_1 \qquad (23)$$

To facilitate calculations of the plastic work done in deforming the blank, the variation of ε_1 with initial radial position is given as, [10]

$$\varepsilon_1 = \varepsilon_m \left[1 - \left(\frac{r}{a}\right)^c\right] \qquad (24)$$

For most purposes c is taken as unity [10] and hence equation (24) is written as

$$\varepsilon_1 = \varepsilon_m \left(1 - \frac{r}{a}\right) \qquad (25)$$

Substituting for ε_1 into equation (23), the representative strain $\bar{\varepsilon}$ is given by

$$\bar{\varepsilon} = 2\varepsilon_1 = 2\varepsilon_m \left(1 - \frac{r}{a}\right) \qquad (26)$$

Thus, the plastic work done is given by

$$W = \frac{2\pi A T_o}{(n+1)} \int_o^a \left[B + \left\{2\,\varepsilon_m \left(\frac{a-r}{a}\right)\right\}\right]^{n+1} r\,dr \qquad (27)$$

After integration, equation (27) is written as

$$W = \frac{2\pi A T_o}{(n+1)} \left[r \left\{ \left(\frac{a}{2\varepsilon_m}\right) \frac{T^{n+2}}{(n+2)} + \left(\frac{a}{2\varepsilon_m}\right)^2 \left(\frac{1}{n+2}\right) \frac{T^{n+3}}{(n+3)} \right\} \right]_{r=a}^{r=o} \qquad (28)$$

where $T = \left[B + \frac{2\varepsilon_m}{a} (a-r) \right]$

Simplyfying the equation (28), we get

$$W = \frac{\pi\, a^2\, T_o\, A}{(n+1)(n+2)(n+3)} \left[\frac{(B + 2\varepsilon_m)^{n+3}}{2\,\varepsilon_m^2} \right] \qquad (29)$$

It is assumed that the kinetic energy E acquired by the blank is due to the impulse delivered by a single shock wave and this is entirely dissipated as the plastic work. Hence, the initial speed of the blank is found by equating the kinetic energy to the plastic work. Hence,

$$\frac{1}{2} \left[\pi\, a^2\, T_o\, (w/g)\right] V_o^2 = \frac{\pi a^2\, T_o A\, (B+2\varepsilon_m)^{n+3}}{2(n+1)(n+2)(n+3)\,\varepsilon_m^2} \qquad (30)$$

The initial speed of the blank V_o is obtained from equation (30) as,

$$V_o = \left[\frac{A\,(B + 2\,\varepsilon_m)^{n+3}}{(w/g)(n+1)(n+2)(n+3)\,\varepsilon_m^2} \right]^{1/2} \qquad (31)$$

2.4.4 Estimation of Explosive Charge Weight

Equation (15) gives a relation between dynamic effective pressure and hydrostatic pressure. Substituting from equations (3), (5), (8), (9), (10), (11), (12), (14), (17), (18) and (31) in equation (15), we get

$$\left[\frac{2A_1\,(W^{1/3}/R_o)}{6.7}^{\alpha_1}\right]\left[2\left\{\frac{\sin k_1 a}{k_1 a} - \frac{(1-\cos k_1 a)}{k_1^2 a^2}\right\}\right]$$

$$= \frac{2\left[A\left\{B+2\ln\left(1+\frac{h^2}{a^2}\right)\right\}^n\right]\left[T_o/e^{2\ln\left(1+\frac{h^2}{a^2}\right)}\right]\left[2\ln\left(1+\frac{h^2}{a^2}\right)\right]}{\left(\frac{h^2+a^2}{2h}\right)\left[2h/\left\{\frac{A\left[B+2\ln\left(1+\frac{h^2}{a^2}\right)\right]^{n+3}}{(w/g)(n+1)(n+2)(n+3)\left[\ln\left(1+\frac{h^2}{a^2}\right)\right]^2}\right\}^{1/2}\right]} \qquad (32)$$

For a given height of deformation equation (32) can be solved to give the weight of explosive charge required W.

CHAPTER III

INSTABILITY IN EXPLOSIVE FORMING

3.1 GENERAL

Instability in a stretch forming process occurs when the stresses and strains reach such a critical value that equilibrium cannot be established between external forces and internal resistance offered by the material i.e. when strain increament occurs without simultaneous increase in stress. It is observed that during stretch forming of elastic-plastic materials, fracture of the sheet metal does not occur abruptly but is preceeded by the loss of stability of the sheet material. [40] As a result, the strain concentration in certain regions of the formed dome takes place depending upon the possibility of occurence of a local discontinuity or initial inhomogeneity in the material. The remaining regions outside the local thinning zone undergo unloading and the plastic strains in these regions start decreasing. With further reduction in thickness of sheet, the discontinuity in the material takes the shape of a groove. With further increase in loading, the groove proceeds in a direction perpendicular to the direction of larger principal stress. The process of local groove formation with reduction in thickness of sheet is known as necking which results in

a loss of cohesion leading to fracture of sheet-material. Limit strains are the strains occuring outside the local necking region at the time of initiation of local necking. In a metal forming process, the limit strain is known to depend upon [49]

(a) mechanical properties of the deformed material

(b) mode of loading

(c) loading history of the process

(d) initial thickness and initial grain diameter of the sheet-material [49]

(e) initial surface roughness of the sheet material and its variation with plastic deformations [49].

Limit strain values are predicted for the case of explosive forming. Some of the above factors are considered in following sections.

3.2 VARIATION OF SURFACE ROUGHNESS WITH PLASTIC DEFORMATION

It was found by Kienzle [46] that the surface roughness of sheet material increases when sheet material is stretched plastically. Osakada and Oyane [47] and Fukuda et al. [48] found that the roughness of a free surface of the material increased approximately in proportion to the magnitude of the generalised strain and the grain diameter. Fukuda et al. [48] expressed

the variation of roughness of free surface as,

$$R = R_o + k d_o \bar{\varepsilon} \qquad (33)$$

where R is the surface roughness at a generalised strain $\bar{\varepsilon}$, R_o is the initial surface roughness and d_o is the initial average grain diameter. k is an empirical constant which is dependent on the crystal lattice structure of the material. Osakada and Oyane [47] found that the rate of increase in roughness is least for materials with body centred cubic structures (V, Ta, α - cr, Mo, α - W etc.) and greatest for materials with hexagonal closed packed structures (Zn, cd, r - T_i etc.) with variation of roughness for face centred cubic materials (Cu, Al, β-N_i, Pt, γ-Fe etc.) falling in between.

3.3 MODEL FOR CHARACTERISATION OF SURFACE ROUGHNESS

Parmar and Mellor [50] characterized the surface roughness by right pyramids as shown in Fig. 5. The stretched rectangular element of the flat sheet has sides L_1 and L_2 and is subjected to tensile forces P_1 and P_2 as shown. The base of the pyramid has sides $(M_1/N_1)\ L_1$ and $(M_2/N_2)\ L_2$ where N_1 and N_2 are the number of grains in length L_1 and L_2 respectively and

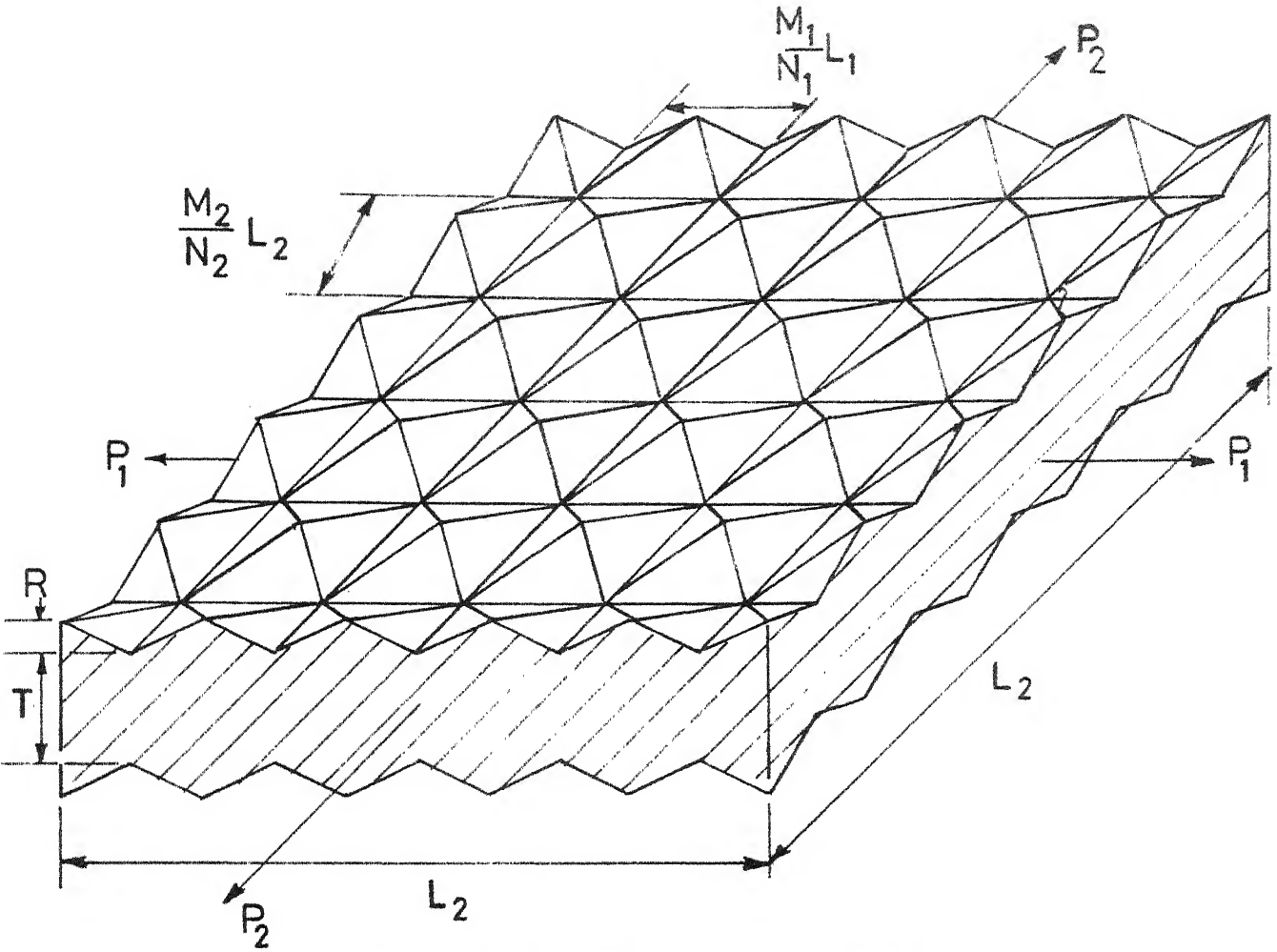

FIG.5 ASSUMED MODEL FOR CHARACTERISATION OF SURFACE ROUGHNESS

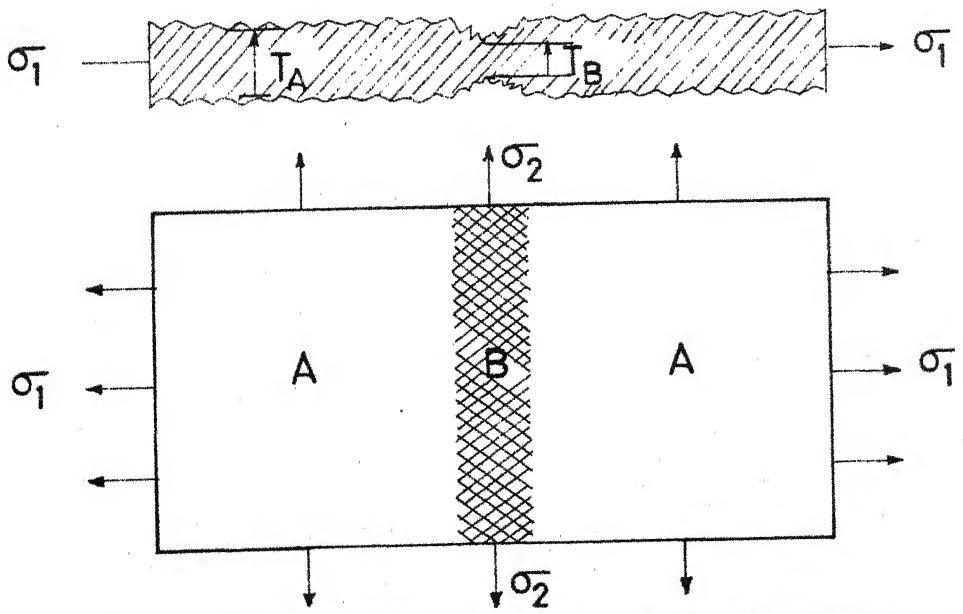

FIG.6 THE MODEL FOR DEFORMATION AFTER

M_1 and M_2 are constants which are introduced to make some allowance for the possibility that a surface roughness peak is not made up simply from a single grain. They further assumed that the load is carried by the minimum thickness of the sheet T. As plastic deformation takes place, the surface roughness increases and it is assumed that the pyramidal shape of the surface asperities persists.

The model therefore describes a system where material leaves the load carrying volume of the metal, as plastic deformation proceeds, thereby, increasing the volume constituting the surface asperities which are assumed not to carry any of the load. Thus, although the total volume of the material within the element can be assumed constant for large plastic strains, the volume of the load carrying material continually decreases with increasing strain.

3.4 ESTIMATION OF INSTABILITY STRAIN IN BIAXIAL TENSION [49]

For biaxial tension $\sigma_2 = x\sigma_1$ and $\sigma_3 = 0$, where x is the stress-ratio. Thus, Levy-Mises equations for the principal directions are written in the form

$$\frac{d\varepsilon_1}{2-x} = \frac{d\varepsilon_2}{2x-1} = -\frac{d\varepsilon_3}{1+x} \qquad (34)$$

The general equation for representative stress $\bar{\sigma}$ and representative strain increament $d\bar{\varepsilon}$ are given by

$$\bar{\sigma} = \sqrt{[(\sigma_1-\sigma_2)^2 + (\sigma_2-\sigma_3)^2 + (\sigma_3-\sigma_1)^2]/2} \qquad (35)$$

$$d\bar{\varepsilon} = \sqrt{2[(d\varepsilon_1 - d\varepsilon_2)^2 + (d\varepsilon_2-d\varepsilon_3)^2 + (d\varepsilon_3 - d\varepsilon_1)^2]/9} \qquad (36)$$

For the case of proportionate biaxial straining, equations (35) and (36) reduce to

$$\bar{\sigma} = \sigma_1 (1 - x + x^2)^{1/2} \qquad (37)$$

$$d\bar{\varepsilon} = d\varepsilon_1 \frac{2}{(2-x)} (1-x + x^2)^{1/2} \qquad (38)$$

From equation (6) the current sheet thickness for a given strain is obtained as

$$T = T_o \exp\left(-\frac{1+x}{2(1-x+x^2)^{1/2}}\bar{\varepsilon}\right) \qquad (39)$$

The thickness given by equation (39) does not, however, include the effect of surface asperities.

Yamaguchi and Mellor [49] worked out the effect of surface asperities, initial thickness and initial grain diameter on the instability strain. They suggested the following instability strain $\bar{\varepsilon}_i$ for an

isotropic material obeying the n-power law of work-hardening,

$$\bar{\varepsilon}_i = \frac{4n(1-x+x^2)^{3/2}}{4-3x-3x^2+4x^3}(f_i)^{1/n} \qquad (40)$$

The thickness parameter f_i is given by,

$$f_i = 1 - \frac{\beta\left(k\frac{d_o}{T_o}\bar{\varepsilon}_i + \frac{R_o}{T_o}\right)}{\exp\left(-\frac{1+x}{2(1-x+x^2)^{1/2}}\bar{\varepsilon}_i\right)} \qquad (41)$$

where,

d_o initial grain diameter

R_o initial surface roughness

x principal stress ratio (σ_2/σ_1)

β A coefficient depending upon the state of contact with tooling. If both sides of the sheet are stretching freely (i.e. not in contact with any tooling) then the value of $\beta = 2$. [49]

It is seen from equation (40) that the value of so obtained instability strain depends upon the grain size, thickness of sheet, rate of increase in surface roughness with plastic strain and the state of contact with tooling. When the effect of surface roughness is not considered, the thickness parameter f_i in equation (40)

becomes unity and equation (40) reduces to the Swift's instability strain equation for a sheet having no local weakness, so that

$$\bar{\varepsilon}_{i_{Swift}} = \frac{4n(1-x+x^2)^{3/2}}{4-3x+3x^2+4x^3} \qquad (42)$$

3.5 APPLICATION OF MARCINIAK-KUCZYNSKI ANALYSIS AT INSTABILITY

Marciniak and Kuczynski [40] assumed that an initial inhomogeneity in the sheet material developes into a groove. As deformation proceeds, the groove deepens and eventually, when plain strain condition ($d\varepsilon_{2B} \rightarrow 0$) is approached in the region of the groove, deformation outside the groove ceases. The representative surface strain outside the groove at this time is termed as the limiting strain ε^*.

Parmar and Meller [50] postulated that at instability a continuous groove, perpendicular to the major principal stress, begins to develop through the troughs of the surface and further straining is concentrated in this groove. They applied the Marciniak-Kuczynski analysis to find out representative limit strain using thickness parameter at instability f_i as obtained from

equation (41). They assumed that the work hardened states both inside and outside the incipient groove depend on the stress state existing in the material upto instability [50]. This means that at instability the material in the incipient groove is slightly more work hardened than the material outside. They [50] assumed that the surface roughness continues to grow after instability.

Between instability and the formation of a localised neck, which indicates the limiting condition, Parmar and Mellor [51] assumed the deformation to be based on Marciniak and Kuczynski [40] analysis. However, they made two modifications when applying the analysis. Firstly, the deformation was assumed to start from the instability condition when the states of work hardening inside and outside the incipient groove are different. They also assumed that the stress-ratio upto instability remains constant and the stress-ratio in the incipient neck is the same as that outside the neck. The state of work hardening inside and outside the neck depends only on the generalised strain existing in these regions at instability. They assumed that current thickness of the sheet depends upon the surface roughness. The process of groove formation is

expressed analytically by the following simultaneous differential equations, [50]

$$\frac{d\bar{\varepsilon}_{1B}}{d\bar{\varepsilon}_B} = \frac{\sqrt{3}}{2}\left\{1 - \frac{(2x-1)^2}{4(1-x+x^2)}\left(\frac{d\bar{\varepsilon}_A}{d\bar{\varepsilon}_B}\right)^2\right\}^{1/2} - \frac{1}{4}\frac{(2x-1)}{(1-x+x^2)^{1/2}}\left(\frac{d\bar{\varepsilon}_A}{d\bar{\varepsilon}_B}\right) \qquad (43)$$

$$\frac{d\bar{\varepsilon}_A}{d\bar{\varepsilon}_B} = \left\{\frac{4(1-x+x^2)}{(2x-1)^2} - \frac{3}{(2x-1)^2}\left[\frac{1}{f_i}\left(\frac{\bar{\varepsilon}_{Ai}+\bar{\varepsilon}_A}{\bar{\varepsilon}_{Bi}+\bar{\varepsilon}_B}\right)^n \left(\frac{T_A/T_{Ai}}{T_B/T_{Bi}}\right)\right]^2\right\}^{1/2} \qquad (44)$$

where,

$\bar{\varepsilon}_{Ai}$ generalized strain in region A at instability

$\bar{\varepsilon}_{Bi}$ generalized strain in region B at instability

f_i thickness ratio at instability (T_{Bi}/T_{Ai})

$\bar{\varepsilon}_A$ generalised strain in region A relative to instability point

$\bar{\varepsilon}_B$ generalised strain in region B relative to instability point

The ratios T_A/T_{Ai} and T_B / T_{Bi} required are obtained from the following equations, [50]

$$\frac{T_A}{T_{Ai}} = \left\{ 1 + \frac{2}{3} \frac{\left[k \frac{d_o}{T_o} \bar{\varepsilon}_{Ai} + \frac{R_o}{T_o} \right]}{(T_{Ai}/T_o)} \right\} \exp \left[\frac{-(1+x)}{2(1-x+x^2)^{1/2}} \bar{\varepsilon}_A \right]$$

$$- \frac{2}{3} \frac{\left[k \frac{d_o}{T_o} (\bar{\varepsilon}_A + \bar{\varepsilon}_{Ai}) + \frac{R_o}{T_o} \right]}{(T_{Ai}/T_o)} \qquad (45)$$

and

$$\frac{T_B}{T_{Bi}} = \left\{ 1 + \frac{2}{3} \frac{\left[k \frac{d_o}{T_o} \bar{\varepsilon}_{Bi} + \frac{R_o}{T_o} \right]}{(T_{Bi}/T_o)} \right\} \exp \left[-\varepsilon_{1B} - \frac{(2x-1)}{2(1-x+x^2)^{1/2}} \bar{\varepsilon}_A \right]$$

$$- \frac{2}{3} \frac{\left[k \frac{d_o}{T_o} (\bar{\varepsilon}_B + \bar{\varepsilon}_{Bi}) + \frac{R_o}{T_o} \right]}{(T_{Bi}/T_o)} \qquad (46)$$

The simultaneous differential equations (43) and (44) can be solved numerically with the aid of a computer. The numerical solution enables the determination of function $\bar{\varepsilon}_A / \bar{\varepsilon}_B$ and hence the strain $\bar{\varepsilon}_A$ at the limiting condition as $d\bar{\varepsilon}_A / d\bar{\varepsilon}_B \to 0$. The limit strain e^* is, now, the sum of the strain that exists upto instability $\bar{\varepsilon}_i$ and the strain $\bar{\varepsilon}_A$ that exists between instability and limiting condition. Thus, limiting strain is given by

$$e^* = \bar{\varepsilon}_i + \bar{\varepsilon}_A$$

CHAPTER IV

EXPERIMENTAL INVESTIGATION

4.1 INTRODUCTION

Rekhi [52] carried out underwater explosive forming tests on 70 - 30 Brass, Aluminium - 1100 and Stainless Steel - 304 sheets of various thickness using Cordtex explosive charge and No. 6 electric ICI detonators. Experimental results of Rekhi regarding profile of formed dome, thickness strains and radial strains are used to verify the theoretical analysis.

Tensile tests are carried out on INSTRON testing machine to obtain stress-strain relationship. Microstructures showing grain boundaries were photographed for different sheet materials used in experimental work of reference [52] to find out average grain diameter d_o. Average surface roughness at various points on different formed domes was measured using profilometer.

4.2 TENSILE TESTS FOR OBTAINING STRESS-STRAIN RELATIONSHIP

Test specimens are prepared according to ISI standards from the sheets of 70 - 30 Brass, Aluminium - 1100 and Stainless Steel - 304 used in explosive forming experiments. Uniaxial tensile tests till fracture are

CHAPTER IV

EXPERIMENTAL INVESTIGATION

4.1 INTRODUCTION

Rekhi [52] carried out underwater explosive forming tests on 70 - 30 Brass, Aluminium - 1100 and Stainless Steel - 304 sheets of various thickness using Cordtex explosive charge and No. 6 electric ICI detonators. Experimental results of Rekhi regarding profile of formed dome, thickness strains and radial strains are used to verify the theoretical analysis.

Tensile tests are carried out on INSTRON testing machine to obtain stress-strain relationship. Microstructures showing grain boundaries were photographed for different sheet materials used in experimental work of reference [52] to find out average grain diameter d_o. Average surface roughness at various points on different formed domes was measured using profilometer.

4.2 TENSILE TESTS FOR OBTAINING STRESS-STRAIN RELATIONSHIP

Test specimens are prepared according to ISI standards from the sheets of 70 - 30 Brass, Aluminium - 1100 and Stainless Steel - 304 used in explosive forming experiments. Uniaxial tensile tests till fracture are

carried out on INSTRON machine. Crosshead speeds in the range of 0.01 cm/min. to 0.05 cm/min. are used for different tests. Load versus extension curves are obtained by a recording system of the machine. Stress and strain values at different stages of tests are computed from the load elongation curves. Stress values are plotted against corresponding natural strain as shown in Figs. 7, 8 and 9. Experimental stress-strain relationships for various materials and their specific weights are shown in Table 1.

TABLE - 1

Sl.No.	Material	Stress-Strain Relationship $= A(B+\bar{\varepsilon})^n$ (kg/mm^2)	Specific Weight ($kg/mm^3 \times 10^{-6}$)
1.	Aluminium-1100	$14.5(0.22 + \bar{\varepsilon})^{0.25}$	2.70
2.	70 - 30 Brass	$64.2\ (0.14 + \bar{\varepsilon})^{0.48}$	8.45
3.	Stainless Steel - 304	$156.5(0.038 + \bar{\varepsilon})^{0.50}$	7.84

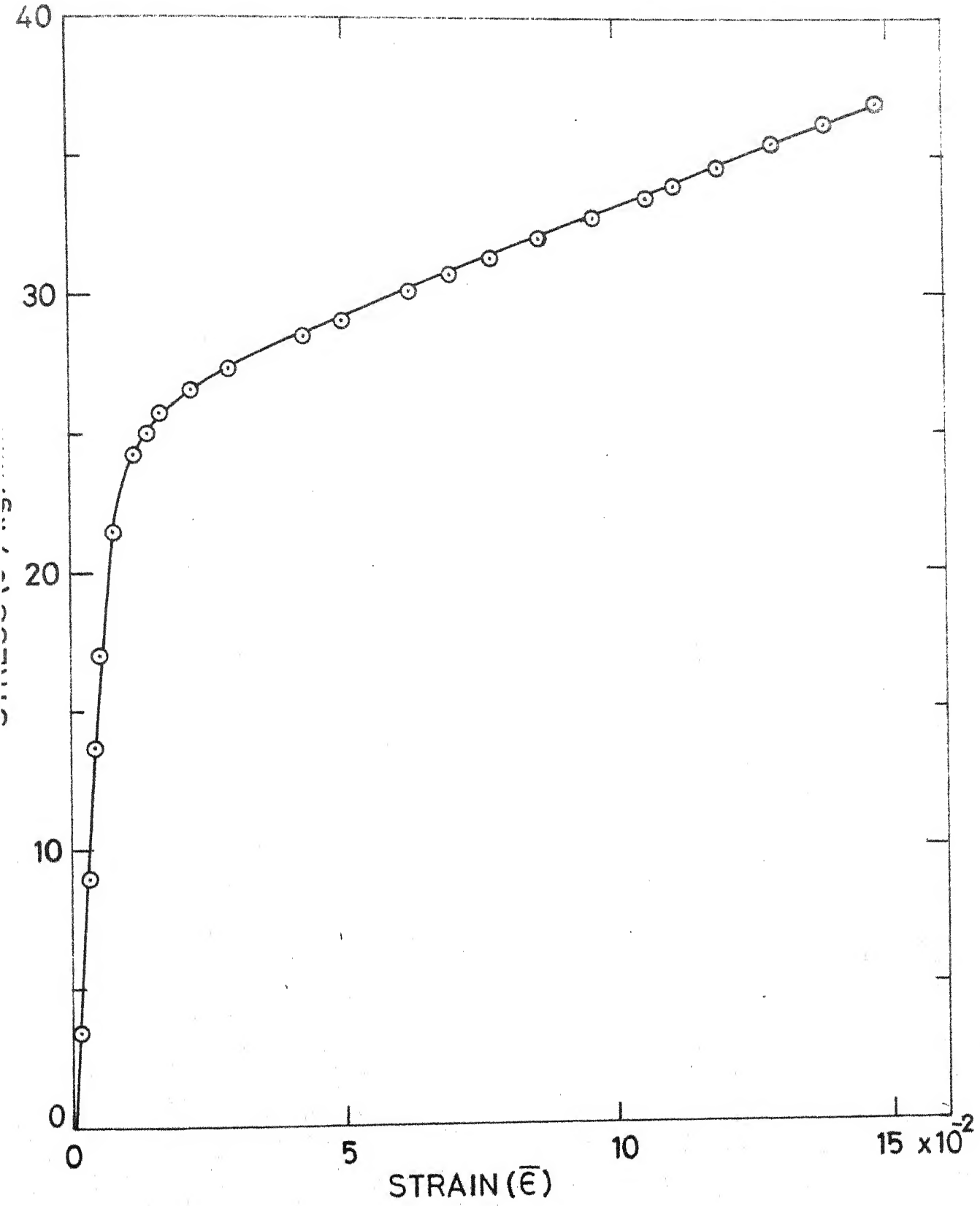

FIG.7 STRESS-STRAIN CURVE FOR 70-30 BRASS

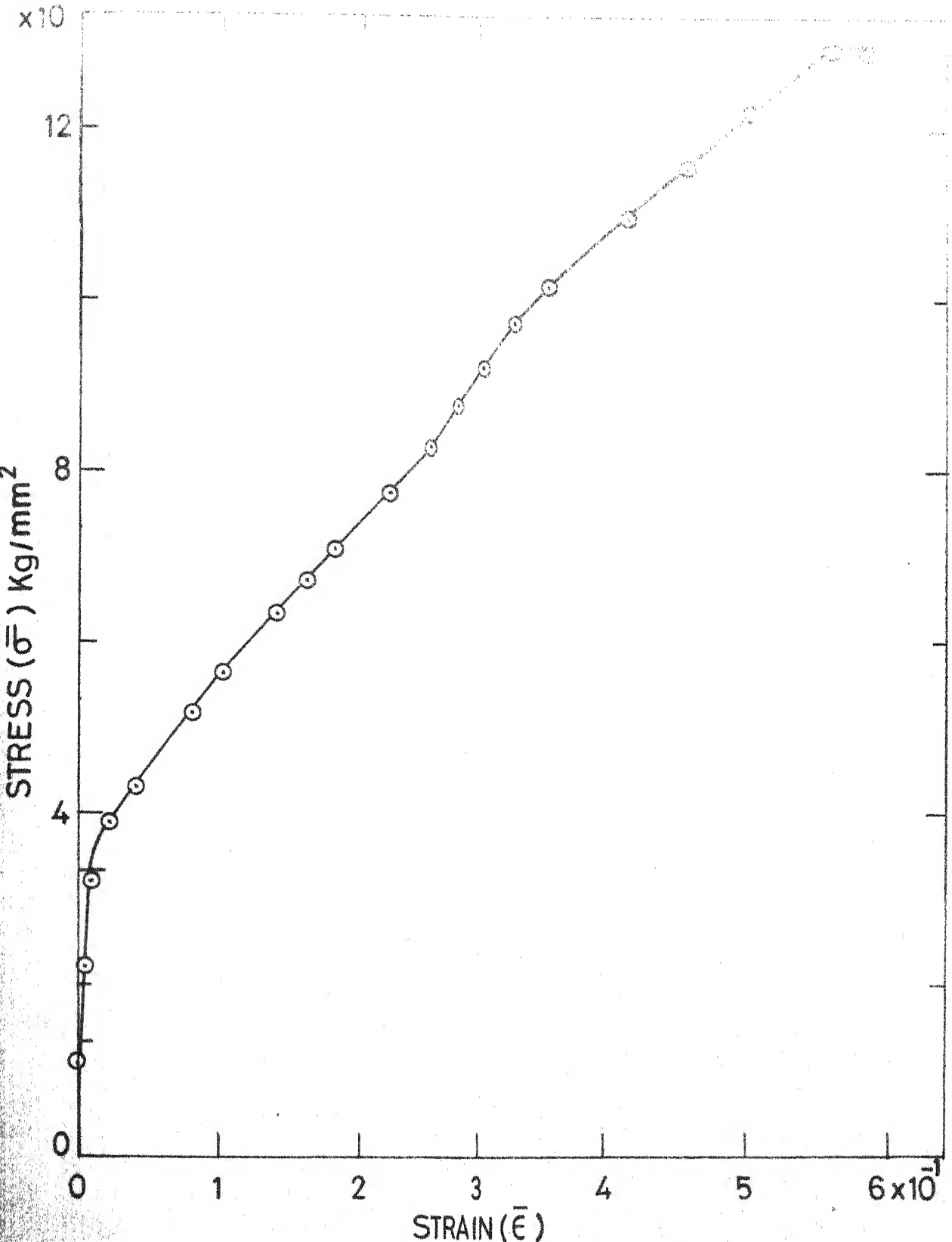

FIG.8 STRESS-STRAIN CURVE FOR STAINLESS STEEL-304

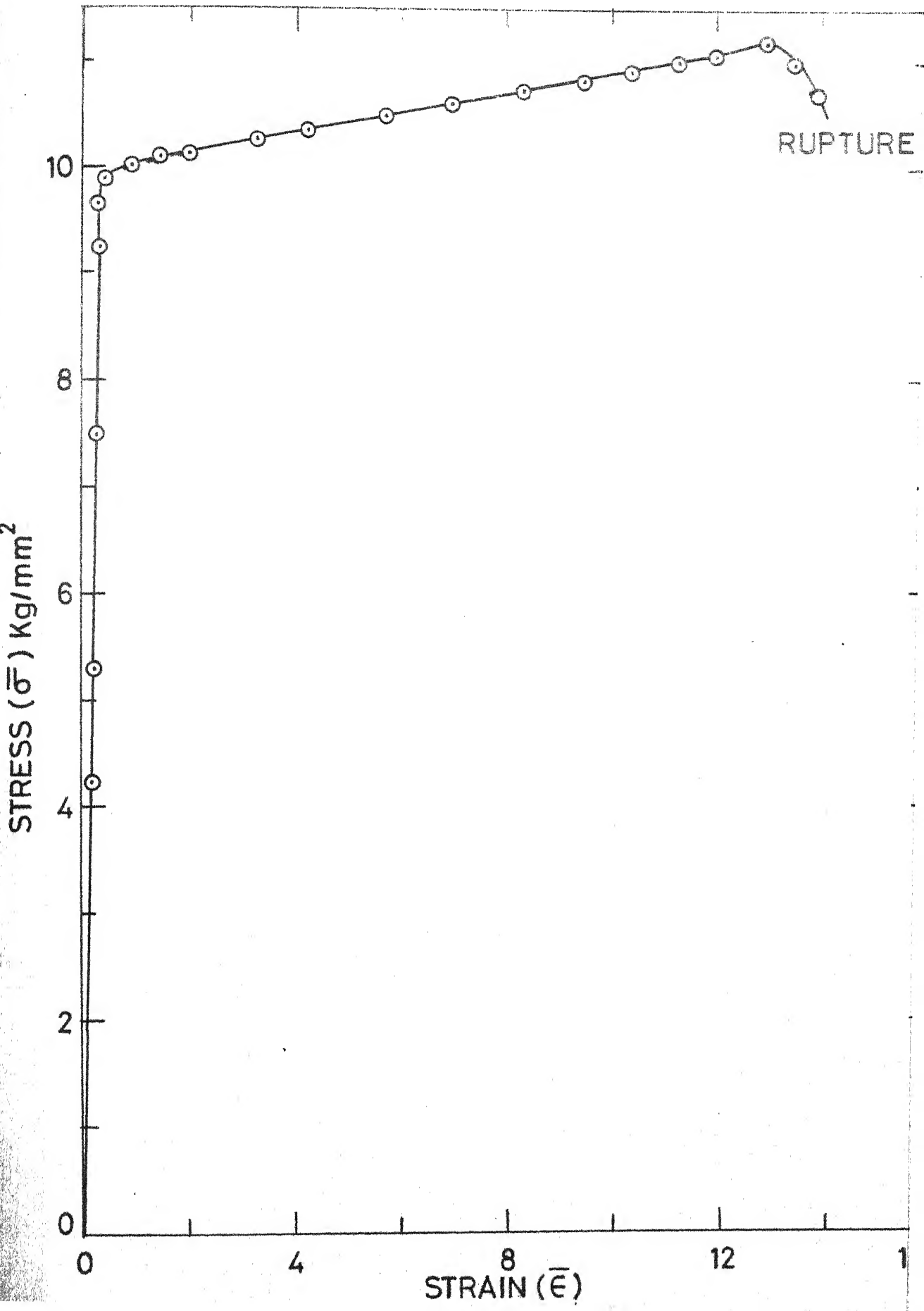
RUPTURE
STRESS ($\bar{\sigma}$) Kg/mm^2
STRAIN ($\bar{\epsilon}$)
0
2
4
6
8
10
0
4
8
12

4.3 MICROSCOPIC EXAMINATION OF SHEET MATERIALS

Micrographic tests are carried out to measure the initial grain diameter in the transverse plane of the sheet materials. The test pieces are prepared by cutting out small specimen of size 10 mm x 5 mm from the sheet materials. These specimens are mounted in a plastic medium and are ground and lapped to give a scratch free polished surface.

To reveal the microstructures, Ferric Cloride solution, 0.5 percent aqueous solution of Hydrofluoric acid and 10 percent aqueous solution of sodium hydroxide are used as echants for 70 - 30 Brass, Stainless Steel - 304 and Aluminium-1100 microsections respectively. Grain boundaries are observed under X400 magnification using metallurgical microscope. Photographs of microstructures are shown in Figs. 10 and 11. The average grain diameter is obtained by counting the number of grains per unit area. The value of average grain diameter are summarised in Table 2. The ratio of initial sheet thickness to initial average grain diameter is plotted in Fig. 12 for various sheet materials of different thicknesses.

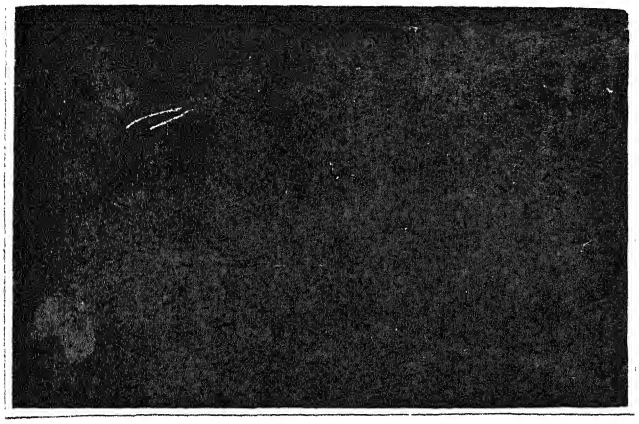

70-30 BRASS
SHEET THICKNESS-0.576 mm

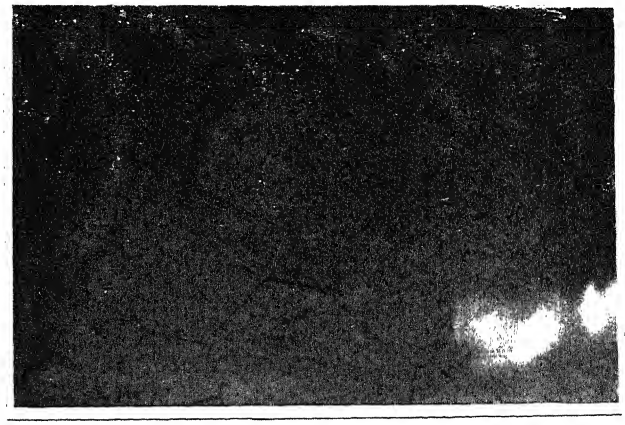

70-30 BRASS
SHEET THICKNESS-0.73 mm

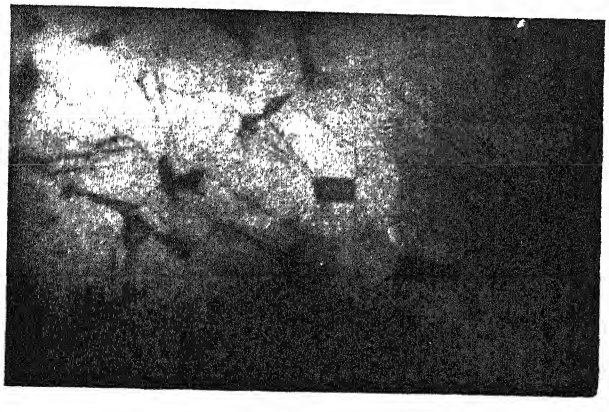

70-30 BRASS
SHEET THICKNESS-1.55 mm

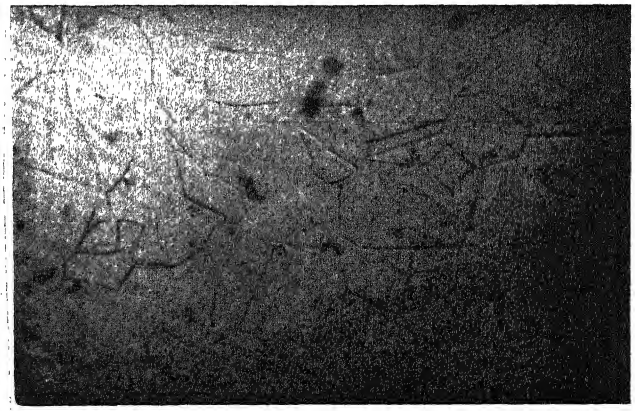

STAINLESS STEEL-304
SHEET THICKNESS-0.875 mm

FIG.10 MICROSTRUCTURES SHOWING GRAIN BOUNDARIES FOR UNDEFORMED SHEETS

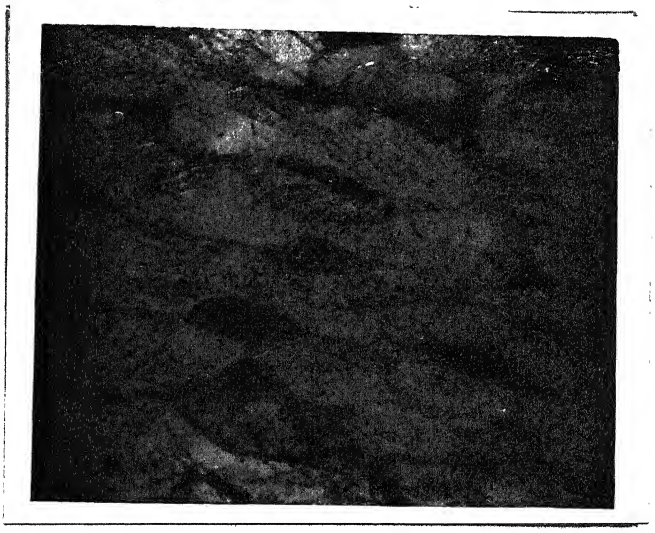

MATERIAL - 70-30 BRASS

SHEET THICKNESS - 0.73 mm

FIG.11 MICROSTRUCTURE SHOWING GRAIN BOUNDARIES AT FRACTURE

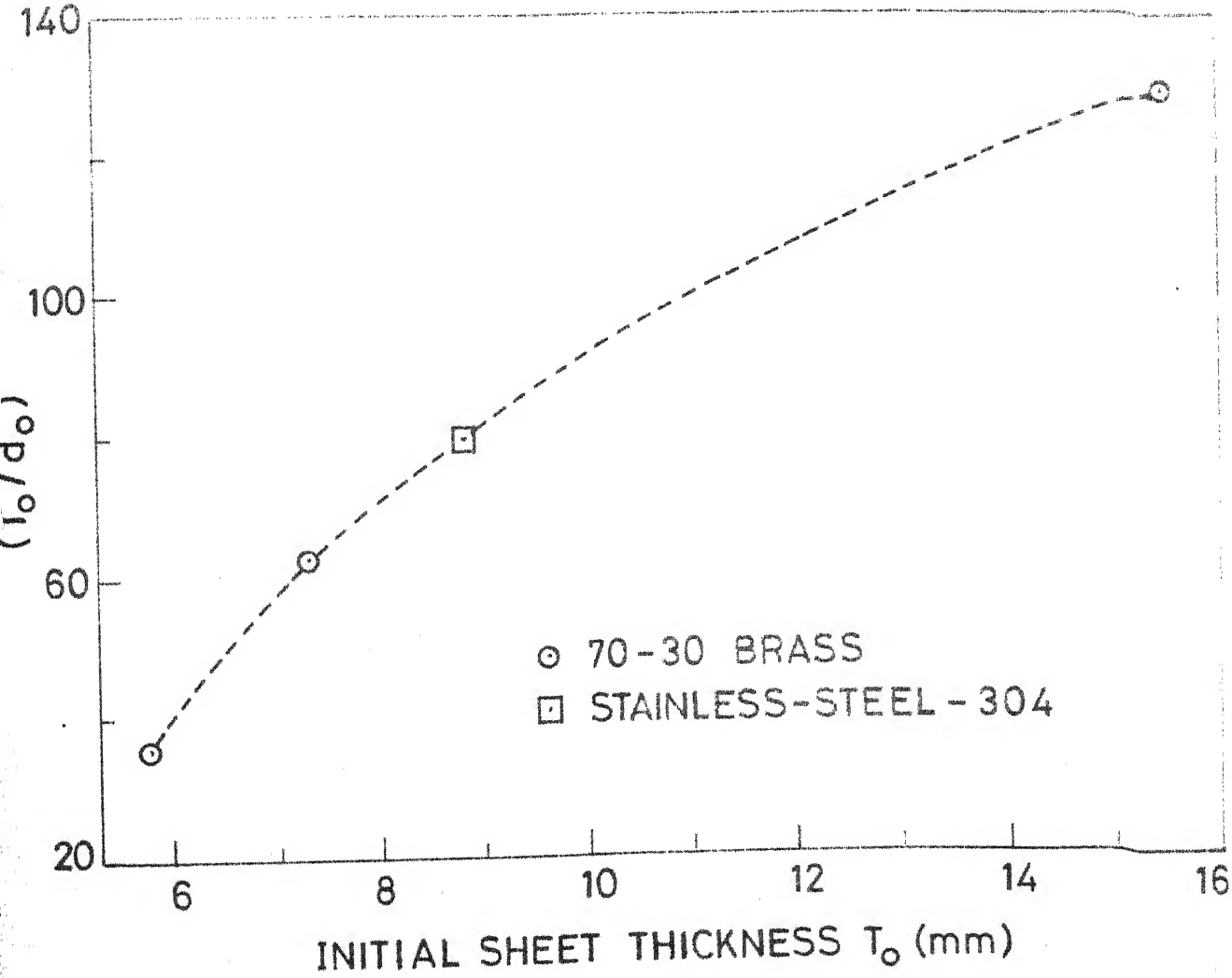

FIG. 12 VARIATION OF RATIO OF INITIAL SHEET THICKNESS TO INITIAL GRA DIAMETER WITH INITIAL THICKNESS OF SHEET.

TABLE - 2

Material	Sheet Thickness (T_o) (mm)	Average Grain Diameter (d_o) (mm) (10^{-3})
70-30 Brass	0.576	14.7
	0.730	11.6
	1.550	12.2
Aluminium-1100	0.671	12.6
	1.189	11.3
	1.610	12.5
Stainless Steel - 304	0.875	11.1

4.4 SURFACE ROUGHNESS MEASUREMENT OF EXPLOSIVELY FORMED DOMES

The surface roughness at various radial positions on explosively formed domes are measured by a profilometer. The ratio of initial surface roughness of sheet material to initial sheet thickness is shown in Table - 3.

TABLE - 3

Material	Sheet Thickness (mm)	R_o / T_o
Aluminium - 1100	0.671	.00116
	1.189	.00077
	1.610	.00067
70 - 30 Brass	0.576	.00104
	0.730	.0008
	1.550	.0004
Stainless Steel-304	0.875	.00112

The variation of surface roughness with experimental representative strain is shown in Fig. 13 for the materials tested. The plots confirm the linear relationship $R = R_o + k\, d_o\, \bar{\varepsilon}$. The experimental values of the constant k are given in Table - 4.

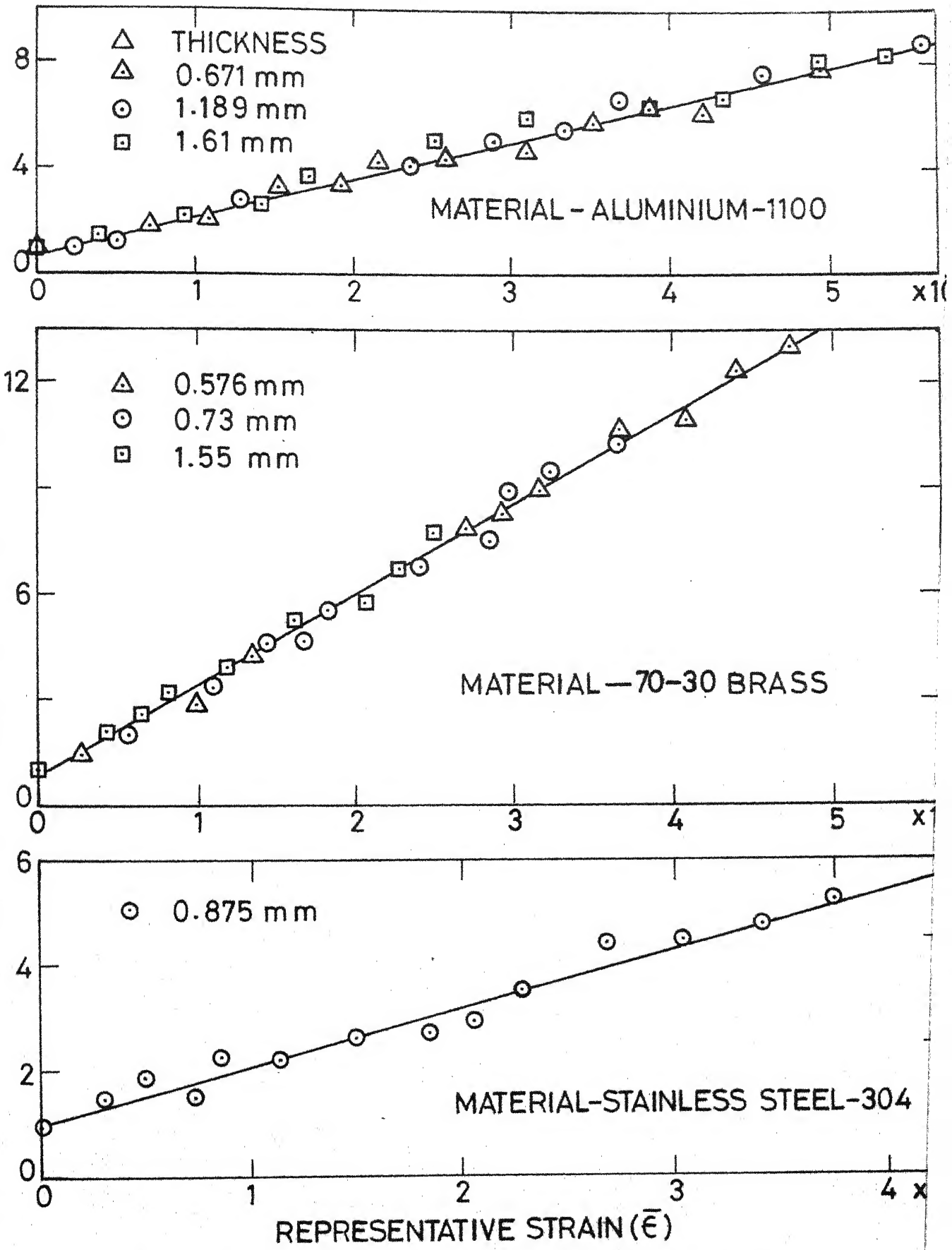

FIG.13 VARIATION OF SURFACE ROUGHNESS

TABLE - 4

Sl.No.	Material	k
1	70 - 30 Brass	1.8
2	Aluminium - 1100	1.2
3	Stainless Steel-304	1.0

CHAPTER V

APPLICATION OF THEORETICAL ANALYSIS TO EXPLOSIVE FORMING

5.1 GENERAL

Theoretical analysis presented in Chapter II and III is applied to the experimental results of Rebbi [52]. The weight of explosive charge required to produce a dome of a given height, material, radius of the blank and sheet thickness is estimated using the theoretical analysis presented in Chapter II . Theoretical predictions are compared with the corresponding experimental values. Fracture conditions are analysed and the limit strains are predicted taking into consideration the effects of i) initial sheet thickness ii) initial grain diameter iii) initial surface roughness and its variation with plastic deformation. The theoretically predicted values of limit strains are compared with corresponding experimental results.

5.2 EVALUATION OF HYDROSTATIC PRESSURE

The hydrostatic pressure required to produce a given deformation, corresponding to experimental conditions [52], are obtained by using hydrostatic bulging theory [39].

In case of hydrostatic bulging, instability occurs at a value of representative strain(which is determined by the properties of the material) followed by fracture at decreasing pressure in the region of pole. Johnson and Mellor [39] plotted the instability strain in hydrostatic bulging against the strain hardening index n for different values of constant 'B' of the stress-strain relationship $\bar{\sigma} = A(B + \bar{\varepsilon})^n$. For the case of hydrostatic bulging the values of instability strains for Aluminium-1100, 70-30 Brass and Stainless Steel - 304 sheets which have been used for explosive forming experiments [39] are 0.50, 0.68 and 0.73 respectively as obtained from the above plot. For harder materials such as Brass and Stainless steel, the strains obtained in explosive forming experiments [52] are below the hydrostatic instability strains. However, for softer materials such as Aluminium, the strains obtained are upto 0.8 which is greater than the hydrostatic instability strain.

For the purpose of calculating effective dynamic pressure, the hydrostatic pressure is assumed constant for strains larger than the hydrostatic instability strain

5.3 EVALUATION OF EFFECTIVE DYNAMIC PRESSURE

Maximum pressure p_m generated by a given weight of

explosive at a given stand-off distance S_o is obtained from equation (3). For Cordtex explosive the constant C, as required in equation (5), is taken as 6.7. [51] The average pressure p_a, as obtained from equation (5), is equal to $p_m/6.7$. The effective dynamic pressure p_d is obtained from equation (14). The value of factor F, which takes into consideration the effect of position of the charge on normal pressure exerted on the sheet, is 0.97 for 150 mm stand-off and 0.92 for 300 mm stand-off. The ratio of dynamic effective pressure to hydrostatic pressure (p_d/p_h) is obtained from equation (15).

5.4 EVALUATION OF STRAIN-RATE AND STRAIN-RATE INDEX

Strain-rate is obtained from equation (18). The value of representative strain $\bar{\epsilon}$, which is required in equation (10), is obtained from equation (9). The initial velocity of deformation, which is required for calculating the time of deformation, is obtained from equation (31). The specific weights of the materials used in equation (31) are given in Table - 1.

The strain-rate index m is obtained from equation (17). The values of strain-rate index are plotted against the height of deformation for 70-30 Brass, Aluminium-1100 and Stainless Steel - 304 in Fig. 14. It

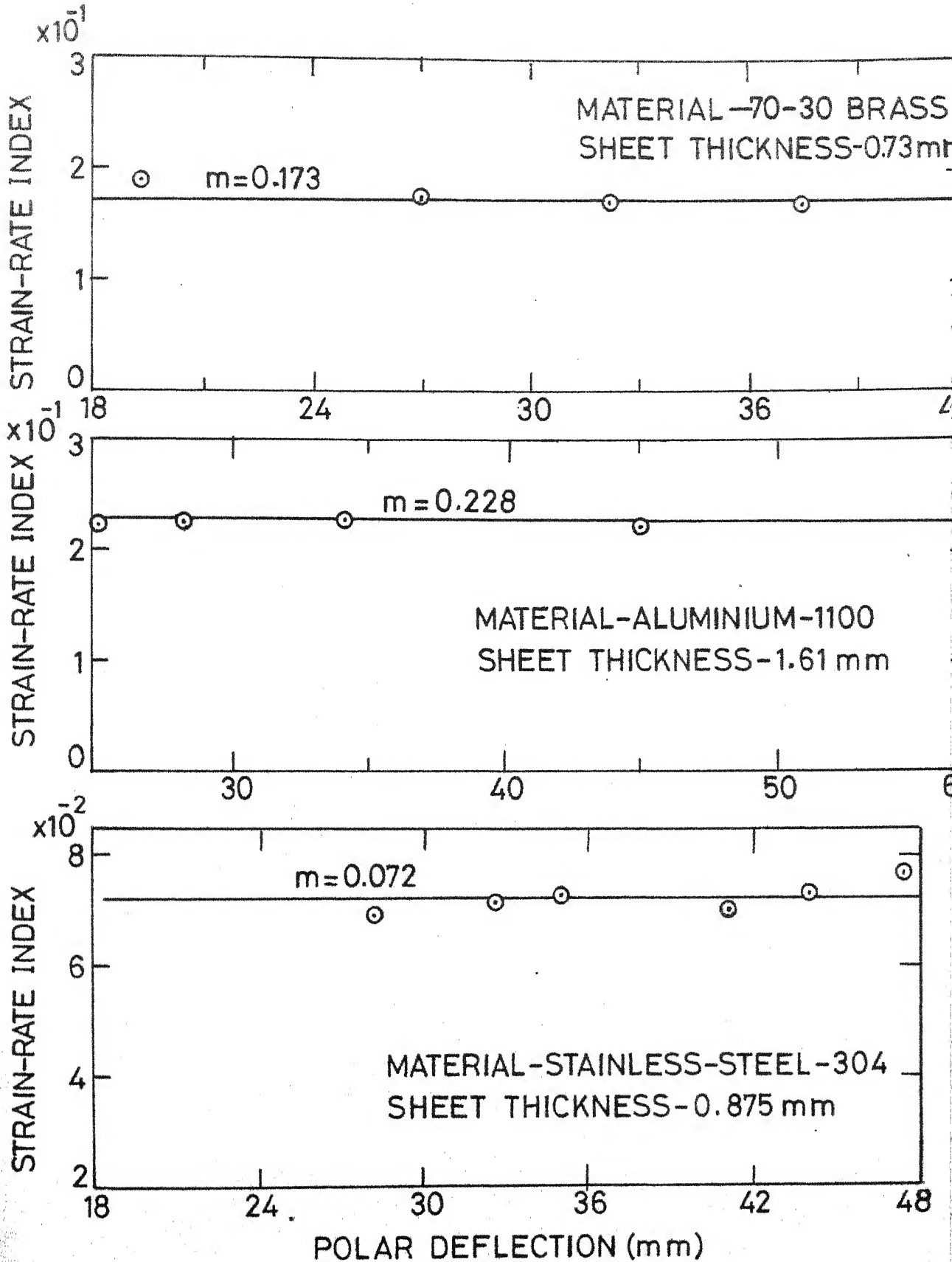

FIG.14 VARIATION OF STRAIN-RATE INDEX (m) WITH POLAR HEIGHT OF DEFORMATION OF DOME

can be seen that strain-rate index m is approximately constant for a particular material. The value of strain-rate index m estimated as 0.228 for Aluminium-1100, 0.173 for 70-30 Brass and 0.072 for Stainless Steel - 304 from explosive forming experiments [52].

5.5 ESTIMATION OF EXPLOSIVE CHARGE WEIGHT

The weight of explosive charge required for a given height of deformation of dome is obtained from equation (32) for a given material, initial sheet thickness, radius of the die and given stand-off distance. The stress-strain data obtained experimentally (as given in Table - 1) are used. The value of strain-rate index, as determined above, is obtained for one thickness of sheet metal. This value of strain-rate index m is used to predict the theoretical charge weight for deformations in sheet materials of other thickness also.

Theoretically predicted charge weights are compared with corresponding experimental values in Figs. 15 to 17. A good agreement between theoretically predicted values and experimental results is observed.

5.6 EVALUATION OF INSTABILITY STRAIN

The value of instability strain $\bar{\varepsilon}_i$ for different sheet materials is obtained from equation (40) taking into

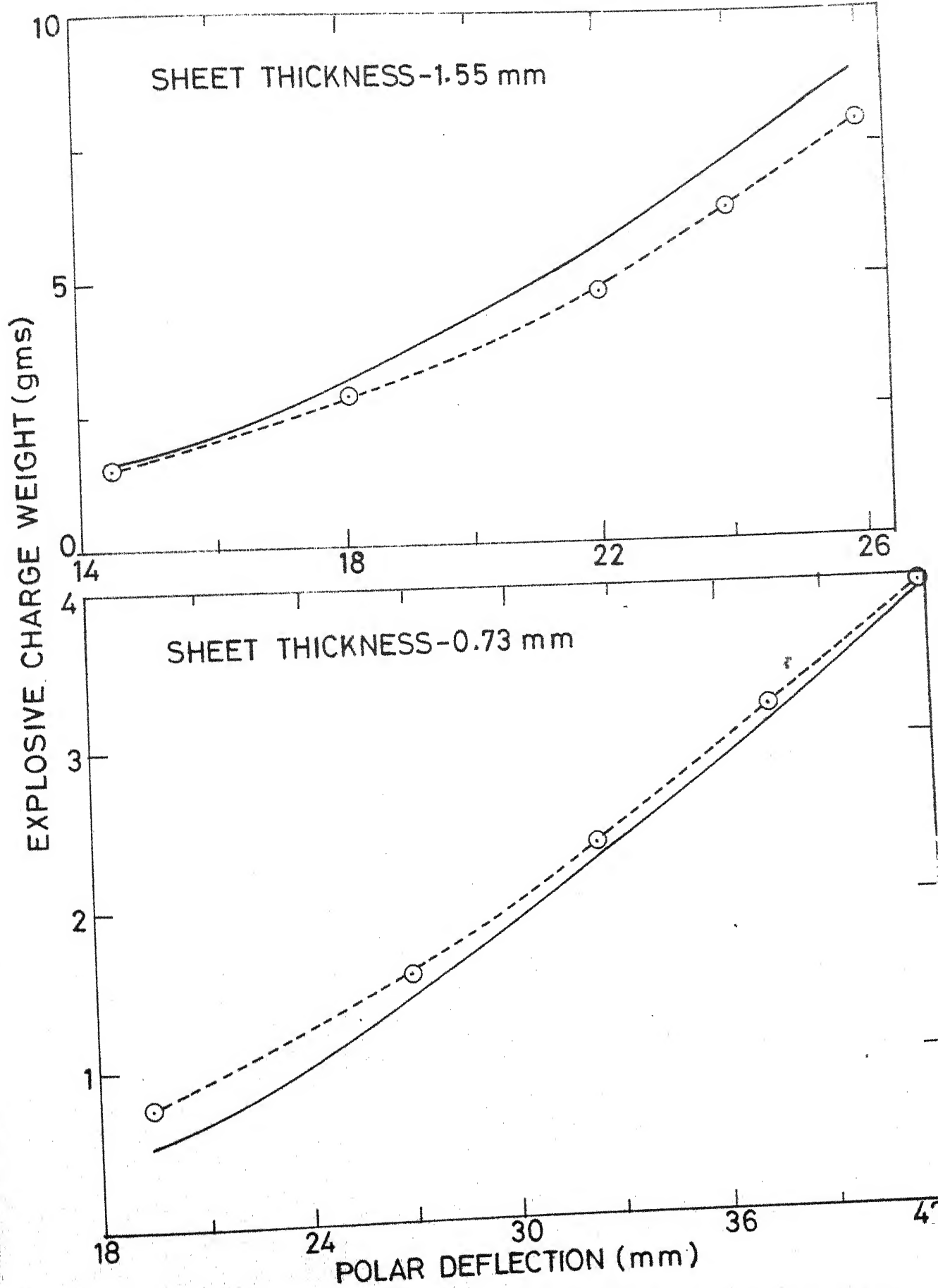

FIG.15 COMPARISON OF THEORETICAL CHARGE

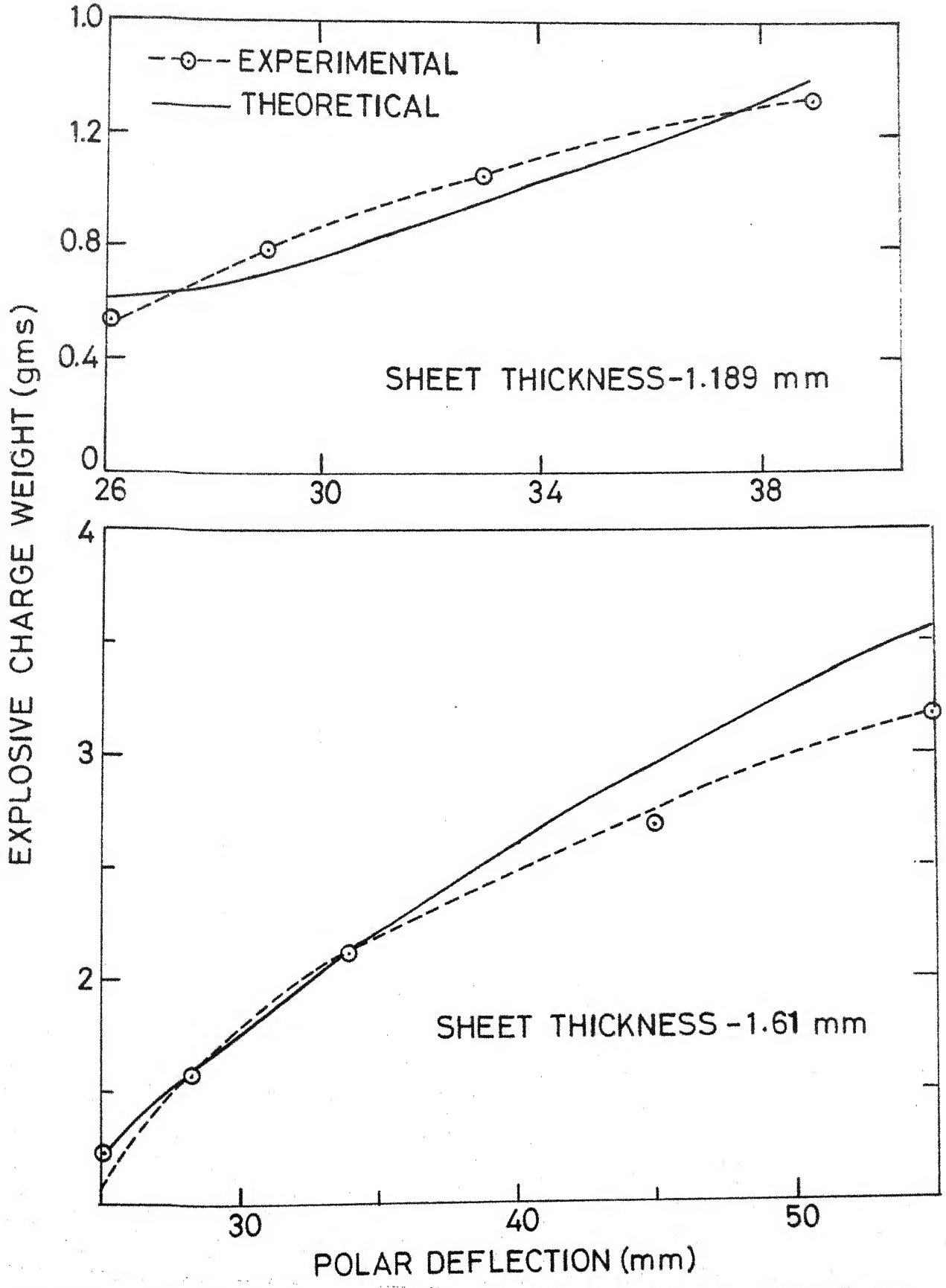

FIG.16 COMPARISON OF THEORETICAL CHARGE WEIGHTS WITH EXPERIMENTAL RESULTS FOR ALUMINIUM-1100

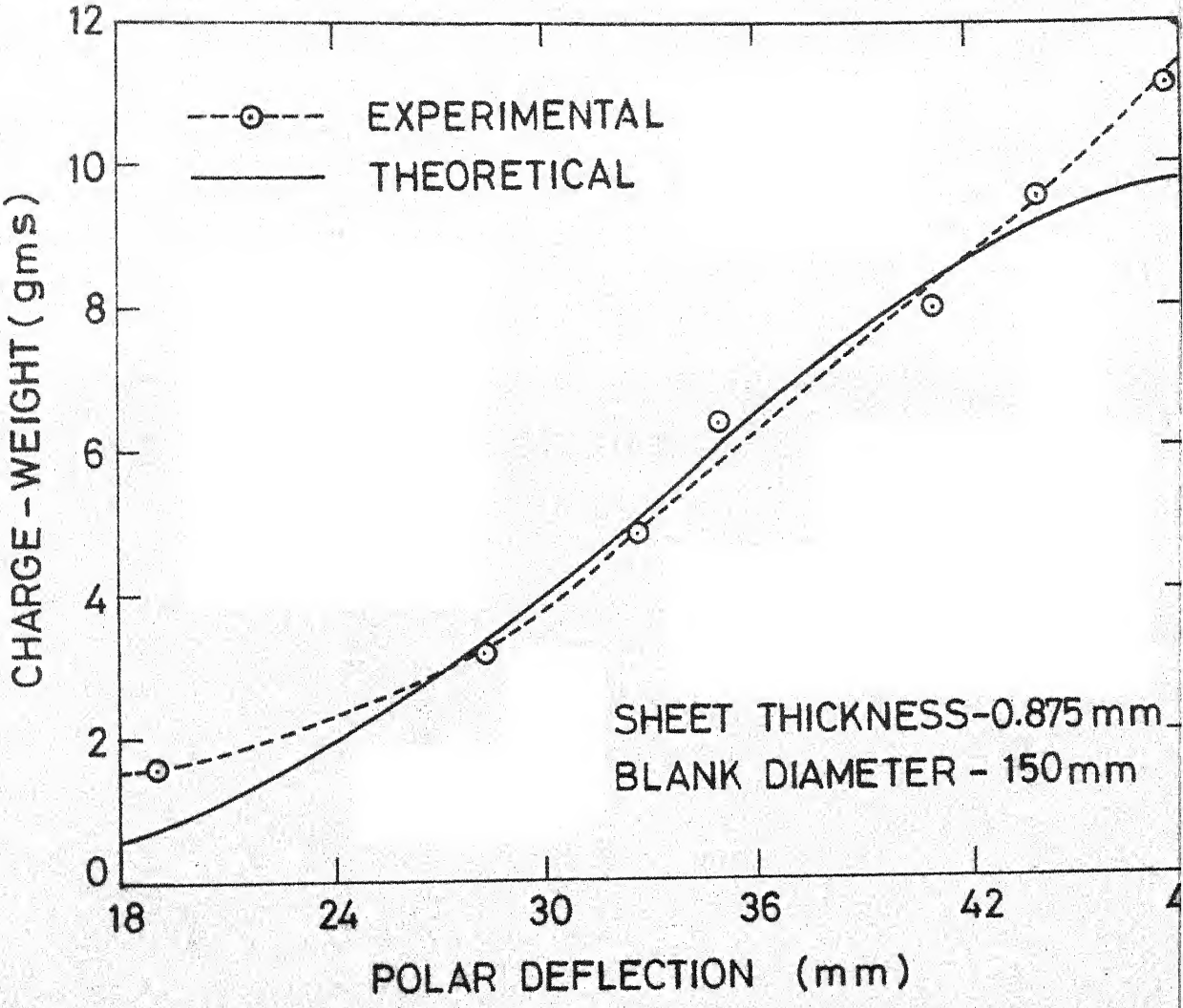

FIG.17 COMPARISON OF THEORETICAL CHARGE WEIGHT WITH EXPERIMENTAL RESULTS FOR STAINLESS STEEEL-30

consideration the effect of surface roughness and the ratio of initial sheet thickness to initial grain diameter.

A FORTRAN IV programme is developed to solve equation (40) numerically by Regula-Falsi method of iterations and to get the instability strain value for different materials. The programme is listed in Appendix I. The R_o/T_o ratios required for solving equation (40) are obtained experimentally and are given in Table - 3. The empirical constant k is taken from Table - 4. The instability strain is plotted against the ratio of initial sheet thickness to initial grain diameter in Figs. 18 and 19 for different materials and stress-ratios in the range of 0.6 to 1.0. The normal Swift instability strain is given by a dashed line. It is seen that the modified instability strains decrease as the ratio T_o/d_o decreases. It is observed from Table-2 that initial grain diameter d_o remains constant for different initial sheet thicknesses of the material. Thus instability strain $\bar{\epsilon}_i$ increases with increase in initial sheet thickness. It is also seen that instability strain increases with increase in stress-ratio.

The thickness parameter at instability f_i is obtained from equation (41) and is plotted in Fig. 20 against

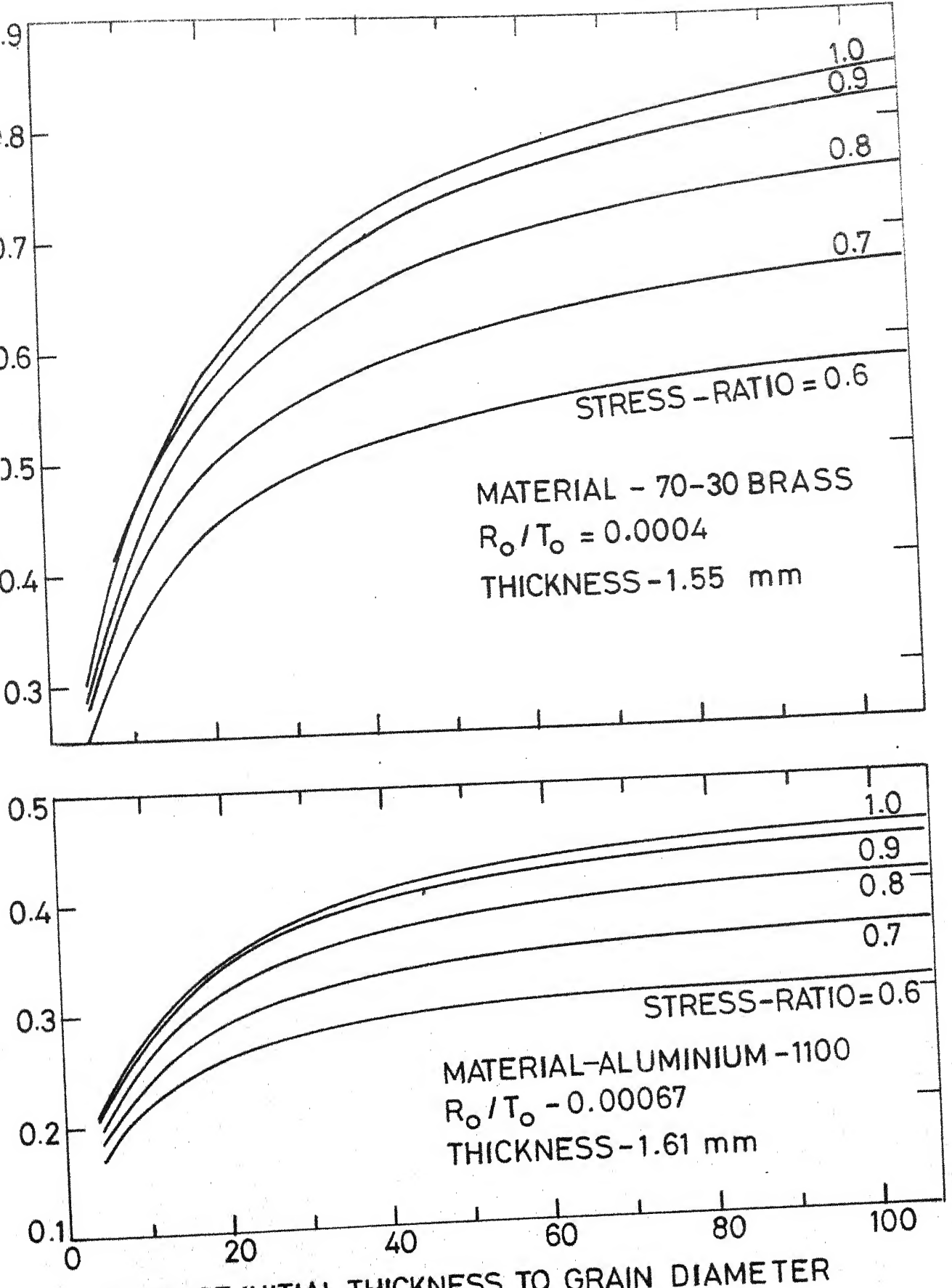

G.18 VARIATION OF INSTABILITY STRAIN WITH RATIO OF INITIAL SHEET THICKNESS TO

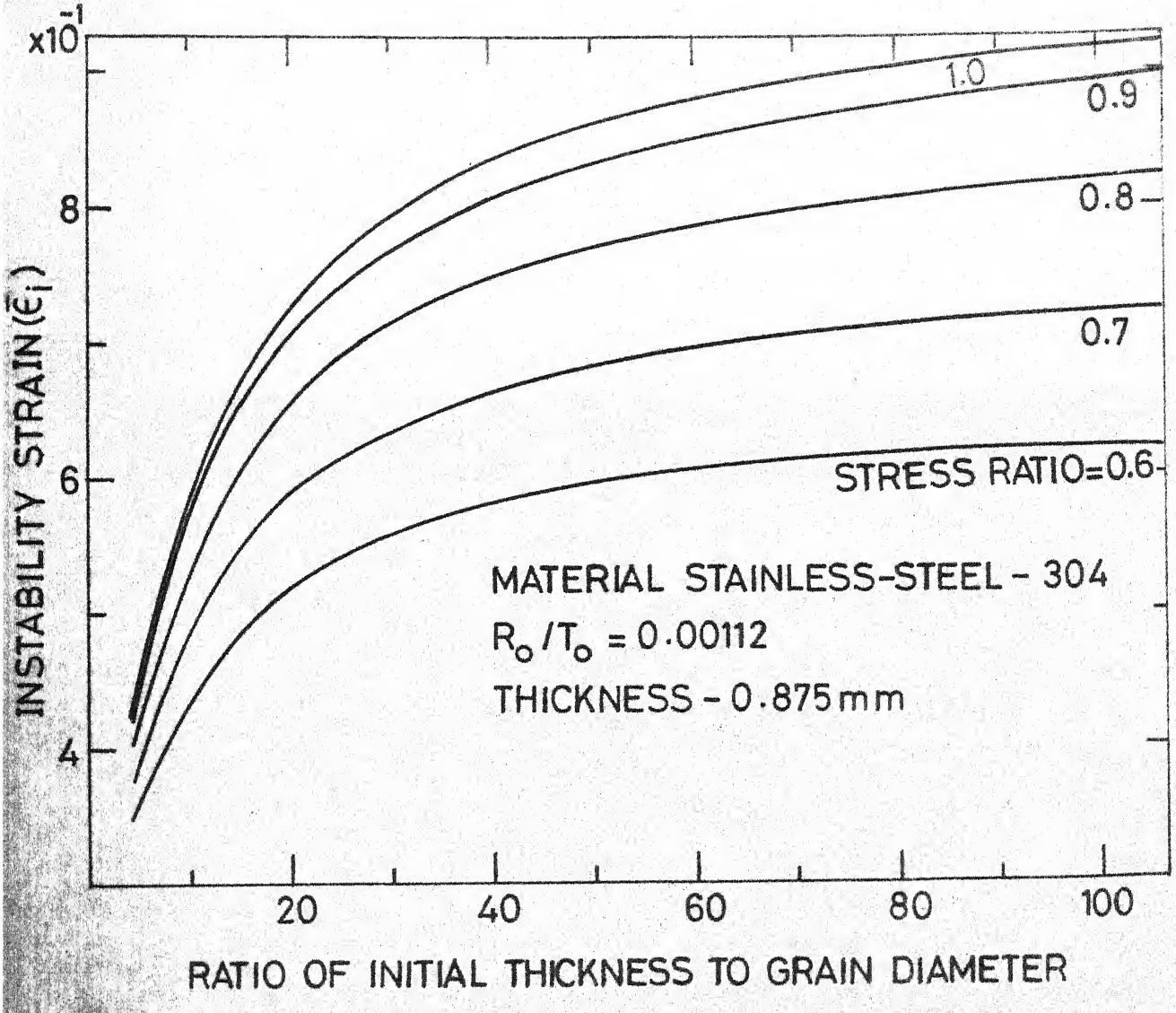

FIG. 19 VARIATION OF INSTABILITY STRAIN WITH RATIO OF INITIAL SHEET THICKNESS TO INITIAL GRAIN DIAMER

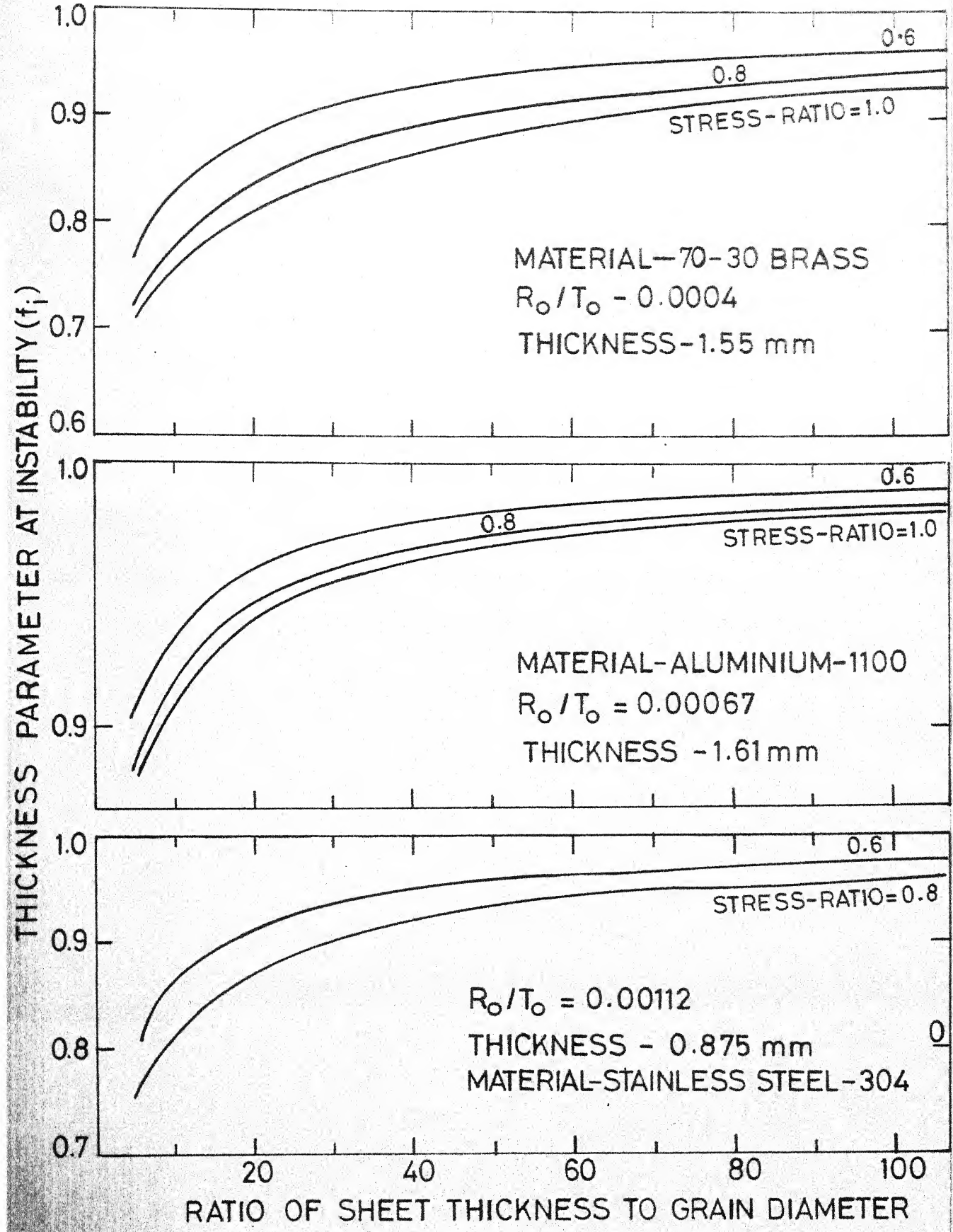

FIG.20 VARIATION OF THICKNESS PARAMETER WITH RATIO OF INITIAL SHEET THICKNESS

the ratio of initial sheet thickness to initial grain diameter for different materials. These values are used latter in the solution of simultaneous differential equations (43) and (44). It is seen from Fig. 20 that thickness parameter at instability increases if the ratio of initial sheet thickness initial grain diameter increases or stress-ratio decreases.

5.7 EVALUATION OF LIMIT STRAINS

Marciniak-Kuczynski analysis is applied at the point of instability to find out the limit strain for the sheet material. The simultaneous differential equations (43) and (44) are solved numerically to determine the strain $\bar{\varepsilon}_A$.

A FORTRAN IV programme is developed to solve the simultaneous differential equations (43) and (44) numerically with the aid of computer. The listing of the programme is given in Appendix - II. The total limit strain is given by $\varepsilon^* = \bar{\varepsilon}_i + \bar{\varepsilon}_A$. The values of limit strains ε^* are plotted against the ratio of initial sheet thickness to initial grain diameter for different materials and different stress-ratios in Figs. 21 to 23. It is observed from the plots that the limit strain increases with increase in sheet thickness. A study of experimental results of explosive forming [52] also shows that

fracture strain increases as the sheet thickness is increased. The fracture strain for Aluminium - 1100 sheet of 0.671 mm thickness is 0.566 while that for thicknesses 1.189 mm and 1.61 mm are 0.778 and 0.803 respectively. Thus, the plots of limit strains are consistent with experimental observations.

5.8 COMPARISON OF THEORETICAL LIMIT STRAIN WITH EXPERIMENTAL RESULTS

Experimental thickness and radial strains are taken from strain versus radial distance plots for explosive forming experiments conducted by Rekhi [52]. It is observed that Aluminium specimens fractured at strain-ratio ($\varepsilon_3/\varepsilon_2$) approximately 2.6 while the strain-ratio ($\varepsilon_3/\varepsilon_2$) near fracture is approximately 3 and 4.25 for 70-30 Brass and Stainless Steel - 304 specimens respectively. The corresponding values of stress-ratio near fracture, as obtained from equation (6), are approximately 0.85 for Aluminium - 1100 and approximately 0.8 and 0.7 for 70 - 30 Brass and Stainless Steel - 304 respectively.

The theoretical representative limit strains for the above materials of different sheet thicknesses are plotted in Fig. 24 along with corresponding experimental values of representative strains for cases of fractured

and unfractured specimens. It is observed from Fig. 24 that theoretically predicted values of limit strain fall between the above two experimental values of representative strain for all the materials.

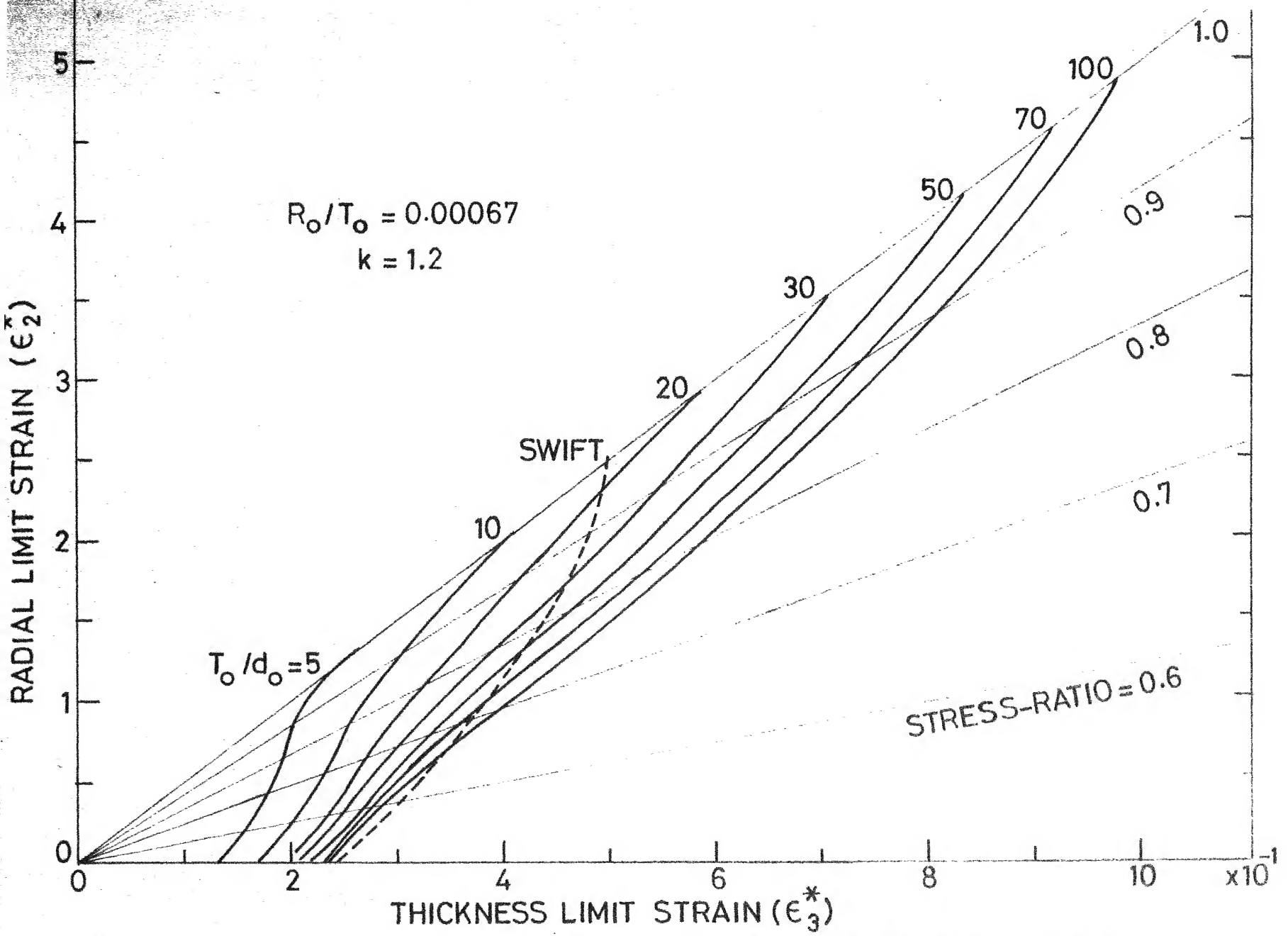

FIG. 21 LIMIT STRAINS FOR ALUMINIUM-1100

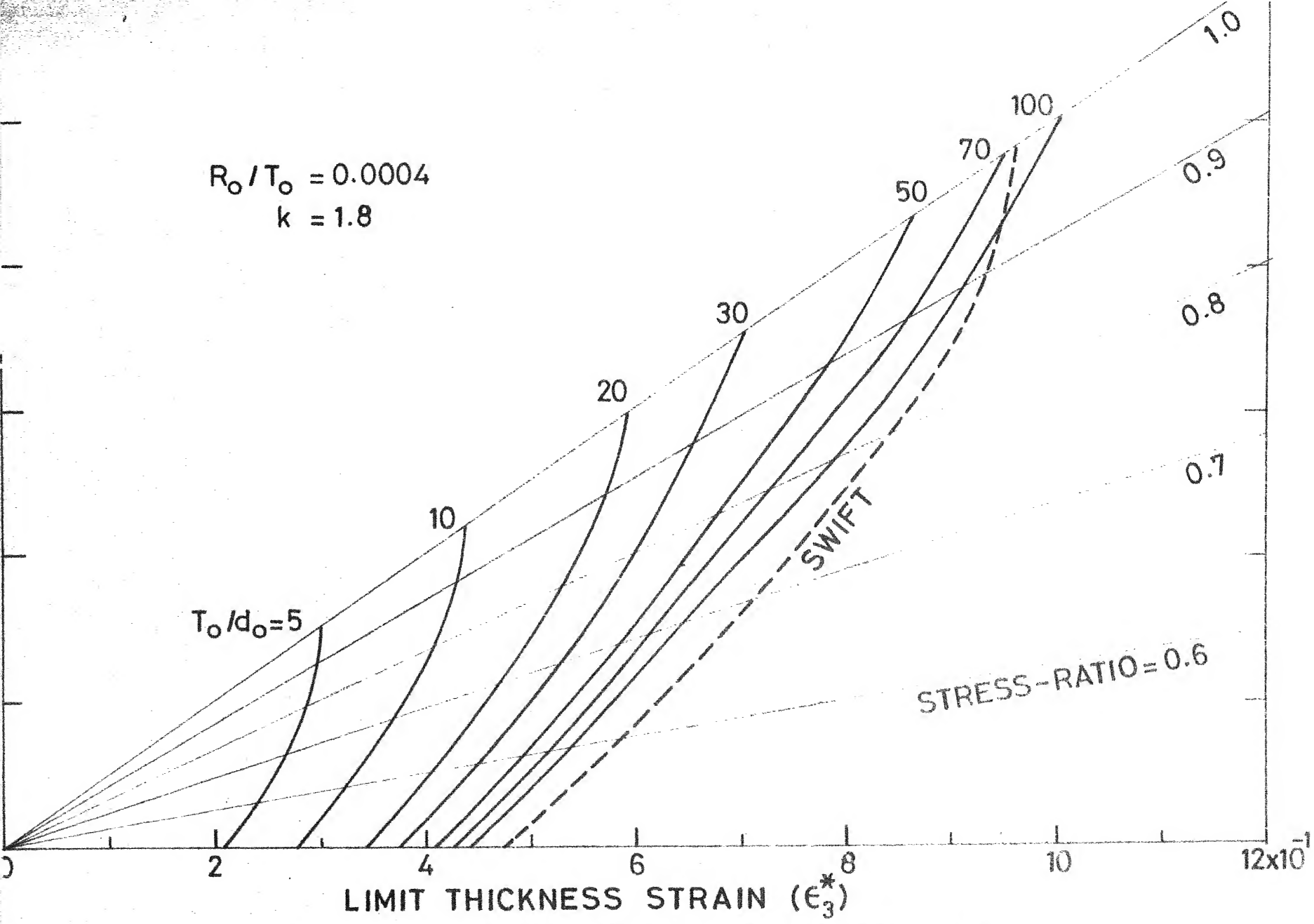

FIG 22 LIMIT STRAINS FOR 70-30 BRASS

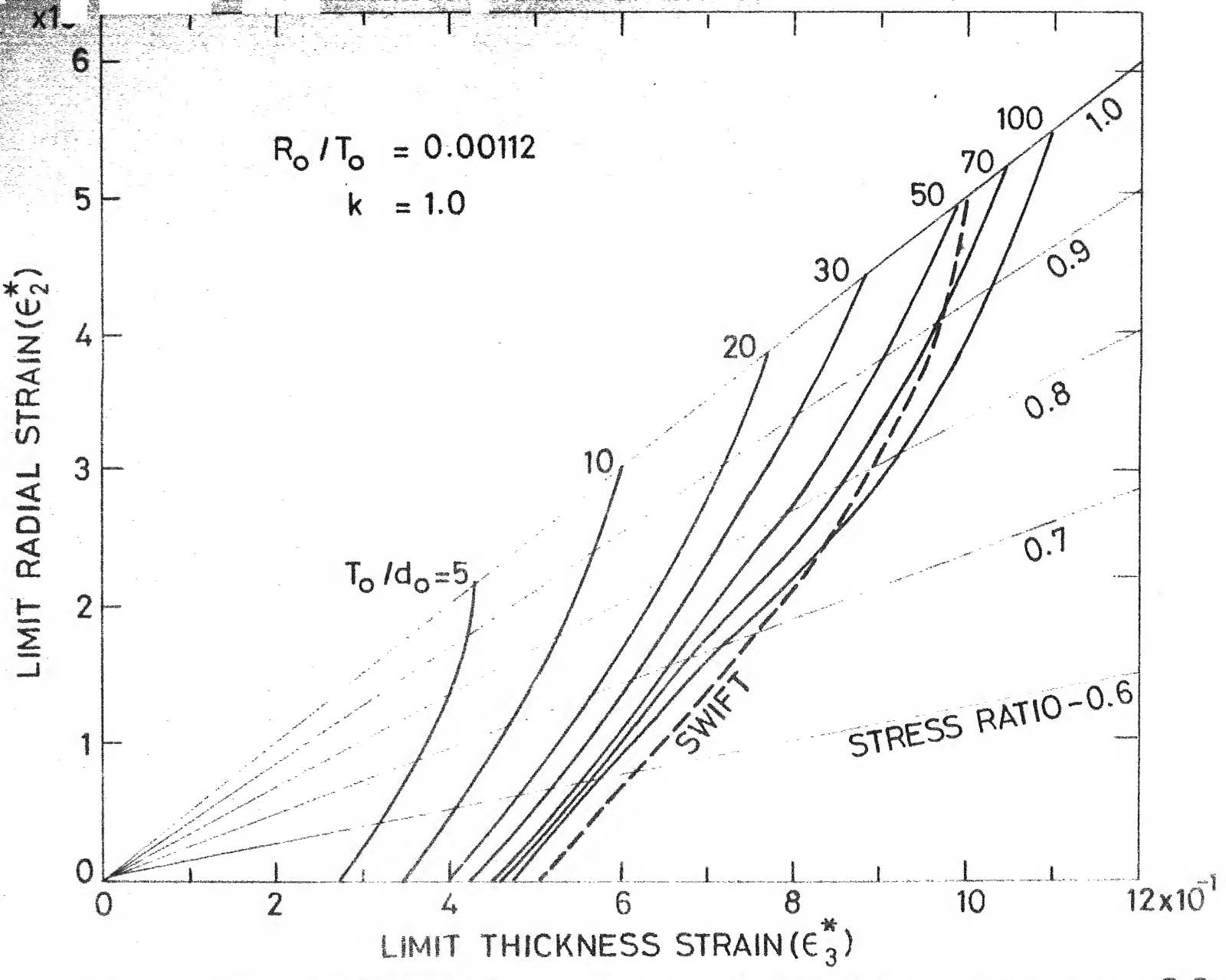

FIG.23 LIMIT STRAINS FOR STAINLESS STEEL-304

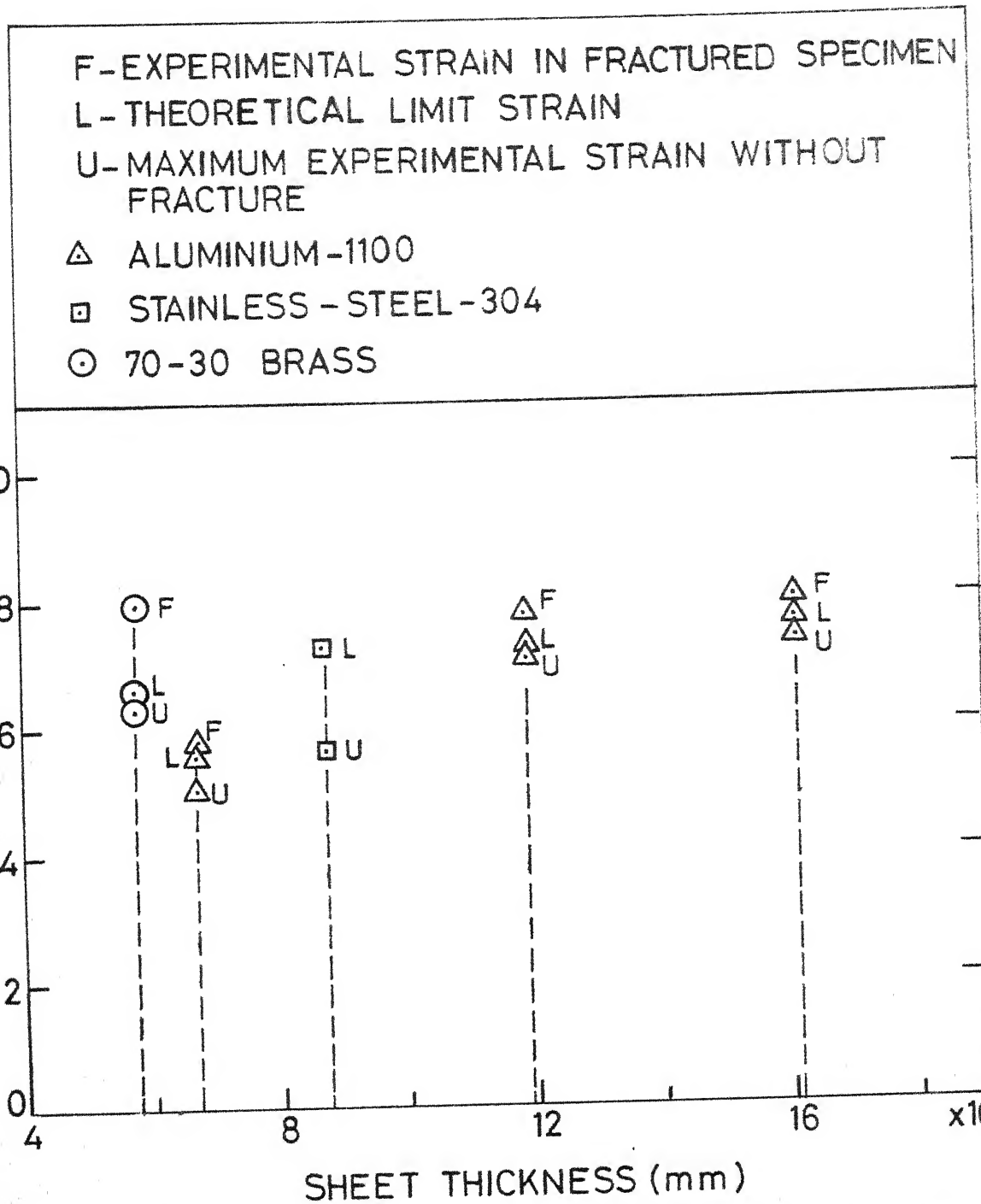

FIG.24 COMPARISON OF THEORETICALLY PREDICTE LIMIT STRAINS WITH EXPERIMENTAL VALUES.

CHAPTER VI

CONCLUSION AND SUGGESTIONS FOR FURTHER WORK

6.1 CONCLUSION

On the basis of results of the present investigation it is concluded that modified analysis of hydrostatic bulging can be applied to explosive forming for the prediction of explosive charge weight provided strain-rate index is known from the material properties. The values of strain-rate index m estimated from the experimental results of explosive forming for Aluminium-1100, 70-30 Brass and Stainless Steel - 304 are 0.228, 0.173 and 0.072 respectively. However, these values need to be verified by independent tests.

Predicted decrease in limit strain with decrease in sheet thickness (Fig. 21 to 23) is consistent with experimental observations.[52] Since theoretically predicted values of representative limit strains fall in between corresponding experimental values of representative strains for the cases of fractured and unfractured specimens, the theoretical analysis holds good for explosive forming.

6.2 SUGGESTIONS FOR FURTHER WORK

(1) High speed stereophotogramatic method can be used to:

(a) analyse the history of deformation process i.e. value of thickness and radial strains at different stages of deformation.

(b) determine the velocity of deformation and strain-rates experimentally.

(2) The stress-ratio x can also be taken into consideration in the analysis of estimation of charge weight. However, it needs extensive study about the variation of stress-ratio with the process parameters.

(3) More work needs to be carried out on surface roughness of sheet materials so as to give the value of empirical constant 'k' in the relation $R = R_o + k \bar{\varepsilon} d_o$ for different material conditions.

(4) The effect of anisotropy can also be considered in the analysis of limit strains.

(a) analyse the history of deformation process i.e. value of thickness and radial strains at different stages of deformation.

(b) determine the velocity of deformation and strain-rates experimentally.

(2) The stress-ratio x can also be taken into consideration in the analysis of estimation of charge weight. However, it needs extensive study about the variation of stress-ratio with the process parameters.

(3) More work needs to be carried out on surface roughness of sheet materials so as to give the value of empirical constant 'k' in the relation $R = R_o + k \bar{\epsilon} d_o$ for different material conditions.

(4) The effect of anisotropy can also be considered in the analysis of limit strains.

REFERENCES

1. C.E. Munroe, 'Modern Explosives', Scribners Magazine, Vol. 3, 1888, p. 563.

2. C.E. Munroe, 'The Applications of Explosives', Popular Science Magazine, Jan., 1900.

3. R.H. Cole, Underwater Explosions, Princeton University Press, Princeton, 1948.

4. W.G. Penny et al., 'A Discussion on Detonation', Proc. of Royal Soc. of London, A 204, 1951, p. 1.

5. J.S. Rinehart and J. Pearson, Explosive Working of Metals, Pergamon Press, London, 1962.

6. W. Johnson and R. Sowerby, 'Experiments on Clamped Blanks Subject to an Underwater Explosive Charge', Proc. I. Mech. E., Vol. 179, Part I, No. 7, 1964-65, p. 197.

7. S.E. Corbett and A.W. Bicker, 'Some Small Scale Experiments in Explosive Forming', Sheet Metal Industries, Vol. 39, No. 423, July 1962, p. 555.

8. N.N. Ida and A.A. Ezra, 'Die-less Explosive Forming of One-piece Thin Shells of Revolution', Proc. 3rd I.M.T.D.R. Conference, Birmingham, 1962, p. 365 (Pergamon).

9. F.W. Travis and W. Johnson, 'Experiments on the Dynamic Deformation of Clamped Circular Sheets of Various Metals

Subjected to an Underwater Explosive Charge, Sheet Metal Industries, Vol. 39, No. 423, July 1962, p. 456.

10. W. Johnson, J.L. Duncan, K. Kormi, R. Sowerby and F.W. Travis, 'Some Contributions to High Rate Sheet Metal Forming', Proc. 4th I.M.T.D.R. Conference, Manchester, Sept. 1963, p. 257 (Pergamon).

11. W. Johnson, A. Poynton, H. Singh and F.W. Travis, 'Experiments in the Underwater Explosive Stretch Forming of Clamped Circular Blank', International Journal of Mechanical Sciences, Vol. 8, No. 4, 1966, p. 237.

12. W. Johnson, K. Kormi and F.W. Travis, 'Explosive Deep Drawing of Circular Blanks Using the Plug Cushion Technique', I.J. Mech. Sc., Vol. 6, No. 4, 1964, p.287.

13. F.W. Travis and W. Johnson, 'Explosives Forming of Cones', Proc. 3rd I.M.T.D.R. Conference, Birmingham, 1962, p. 341 (Pergamon).

14. S.Chatterji and F.W. Travis, 'Effect of Varying Workpiece Thickness on Efficiency of Energy Transfer, Proc. 11th I.M.T.D.R. Conference, 1970, p. 901.

15. G.E. Hudson, 'A Theory of the Dynamic Deformation of a Thin Diaphragm', Journal of Applied Physics, Vol. 22, 1951, p. 1.

16. A.A. Ezra, 'The Effect of Stand-off Distance on the Explosive Forming of Metal Blanks', Paper SP 64-113, High Energy Rate Forming Seminar, American Society of Tool and Manufacturing Engineers, Chicago, 1964.

17. A.A. Ezra, 'Principles and Practices of Explosive Forming', Proc. 5th I.M.T. D.R. Conference, Birmingham, 1964 (Pergamon).

18. G.S. Kainth and M.B.S. Rekhi,'An Experimental Investigation into Explosive Forming of Sheets', Proc. 8th All India Machine Tool Design and Research Conference, 1978, p. 483.

19. A.A. Ezra and F.A. Penning, 'Development of Scaling Laws for Explosive Forming', Experimental Mechanics, Vol. 2, No. 8, 1962, p. 234.

20. C.F. Noble and P.L.B. Oxley, 'Estimating Charge Size in Explosive Forming of Sheet Metal', Proc. 5th I.M.T.D.R. Conference, Birmingham, 1964, p. 329.

21. J.S. Rinehart and J. Pearson, Behavior of Metals Under Impulsive Loads, Dover Publications, 1965.

22. P.W. Bridgman, The Physics of High Pressure, G. Bell and Sons, London, 1949.

23. P.W. Bridgman, Studies in Large Plastic Flow and Fracture, McGraw-Hill Book Company, New York, 1952.

24. D.S. Clark and D.S. Wood, 'The Tensile Impact Properties of Some Metals and Alloys', Transactions, American Society for Metals, Vol. 42, 1950, p. 45.

25. D.W. Ginns, 'The Mechanical Properties of Some Metals and Alloys Broken at Ultra High Speed', Journal of Institute of Metals, Vol. 61, 1937, p. 61.

26. D.S. Clark, 'The Behaviour of Metals Under Dynamic Loading', Trans. American Soc. for Metal, Vol. 46, 1954, p. 34.

27. R.G. Crum and F.T. Mavis, 'Behaviour of Certain Alloys Subjected to Dynamic Loading', Proc. American Soc. for Testing Materials, July 1958, p. 88.

28. F.W. Warnock and J.B. Brennan, 'The Tensile Yield Strength of Steels Under Suddenly Applied Loads', Proc. I. Mech. E., Vol. 159, 1948, p. 1.

29. E.A. Davis, 'The Effect of the Speed of Stretching and the Rate of Loading on the Yielding of Mild Steel', Journal of Applied Mechanics (Trans. ASME), Vol. 60, 1938, p. A-137.

30. H.C. Mann, 'High-Velocity Tension-Impact Tests', Proc. American Soc. for Testing Materials, Vol. 36, Part 2, 1936 p. 85.

31. John Hopkinson, 'On the Rupture of Iron Wine by a Blow', Proc. of Manchester Literary and Philosophical Society, Vol. 11, 1872, p. 40.

32. M.J. Manjoine, 'Influence of Rate of Strain and Temperature on Yield Stress of Mild Steel', Journal of Applied Mechanics (Trans. A.S.M.E.), Vol.66, 1944, p. A-211.

33. A.C. Whiffin, 'The Use of Flat-Ended Projectiles for Determining Dynamic Yield Stress', Proc. of Royal Society, London, Vol. 194A, 1948, p. 300.

34. E.R. Parker and C. Ferguson, 'The Effect of Strain-Rate Upon the Tensile Impact Strength of Some Metals', Transactions, American Society for Metals, Vol. 30, 1942, p. 68.

35. A. Nadai and M.J. Manjoine, 'High Speed Tension Tests at Elevated Temperatures, J. of App. Mech. (Trans. A.S.M.E.) Vol. 63, 1941, p. A-77.

36. J.E. Johnson, D.S. Wood and D.S. Clark, 'Dynamic Stress-Strain Relations for Annealed 2S Aluminium Under Compression Impact ', Journal App. Mechanics, Vol. 20, 1953, p. 523.

37. C.E.N. Sturgess and A.N. Bramley, 'The Use of Impact Forming Devices to obtain Dynamic Stress-Strain Data', Proc. of 11th Int. MTDR Conf., 1970, p. 803.

38. J.D. Compbell and J. Duby, 'The Yield Behaviour of Mild Steel in Dynamic Compression', Proc. Roy. Soc. of London, Vol. 236A, 1956, p. 24.

39. W. Johnson and P.B. Mellor, Engineering Plasticity, Van Nostrand, 1973.

40. Z. Marciniak and K. Kuczynski, 'Limit Strains in the Process of Stretch-Forming Sheet Metal', Int. J. Mech. Sci., Vol. 9, 1967, p. 609.

41. S.P. Keeler and W.A. Backofen, 'Plastic Instability and Fracture in Sheets Stretched Over Rigid Punches', Trans. Am. Soc. Metals., Vol. 36, 1963 , p. 25.

42. Z. Marciniak, K. Kuczynski and T. Pokora, 'Influence of the Plastic Properties of A Material on the Forming Limit Diagram For Sheet Metal in Tension', Int. J. Mech. Sci., Vol. 15, 1973, p. 789.

43. A.K. Ghosh and S.S. Hecker, Proc. 2nd North Am. Metal-working Conf., Wisconsion, June (1974).

44. S. Miyano, J. Japan Soc. Technol. Plasticity, Vol. 1, 1960, p. 335.

45. H. Van Minh, R. Sowerby and J.L. Duncan, 'Probabilistic Model of Limit Strains in Sheet Metals', Int. J. Mech. Sci., Vol. 17, 1975, p. 339.

46. O. Kienzle and K. Mietzner, Atlas Umgeformter Metallischer Oberflachen, 1967.

47. K. Osakada and M. Oyane, Trans. J.S.M.E., Vol. 36, 1970, p. 1017.

48. M. Fukuda, K. Yamaguchi, N. Takakura and Y. Sakano, J. Japan Society Technol. Plasticity, Vol. 15, 1974, p. 994.

49. K. Yamaguchi and P.B. Mellor, 'Thickness and Grain Size Dependence of Limit Strains in Sheet Metal Stretching', Int. J. Mech. Sci., Vol. 18, 1976, p. 85.

50. A. Parmar and P.B. Mellor, 'A New Model for the Prediction of Instability and Limit Strains in Thin Sheet Metal', Int. J. Mech. Sci., Vol. 19, 1977, p. 389.

51. F.W. Wilson, High Velocity Forming of Metals, ASTME Publication, Prentice Hall International, London (1964).

52. M.B.S. Rekhi, 'An Experimental Investigation into Explosive Forming of Sheets', M.Tech. Thesis, Mech. Engg. Department, I.I.T. Kanpur.

APPENDIX I

```
C
C     ....FINDING INSTABILITY STRAIN USING REGULA FALSI..................
      DIMENSION AZB6(50,2,100),NN(10)
      R1=5.0
      READ*,SR,P,BETA,CONS,R2,XL,XR,EPS,ITMAX,NO,KSR
      [illegible] R1,SR,P,BETA,CONS,R2
      PRINT*,SR,P,BETA,CONS,R2,XL,XR,EPS,ITMAX,NO,KSR
      DO20N=1,KSR
      PRINT15
15    FORMAT(/'==================================================',/)
      PRINT16,SR
16    FORMAT(1H0,5X,'THE VALUE OF STRESS RATIO=',F8.3//)
      PRINT18
18    FORMAT('==================================================')
      PRINT99
99    FORMAT(3X,'(TH/DO)',3X,'ITER',8X,'X2',12X,'EH',13X,'ER',13X,'ET
     1',9X,'FI',7X,'CORR',6X,'FX2',4X,'CF')
      DO20J=1,NO
C
C     ....EVALUATE F. AT THE ENDS OF INTERVAL ............
      CALL VAJ(XR,STR)
      FXR=STR
      CALL VAJ(XL,STR)
      FXL=STR
C
C     ....CHECK FOR PRESENCE OF A ROOT....................
      IF(FXL*FXR)5,3,2
2     PRINT201
201   FORMAT(20X,'POSSIBLY NO ROOT ON STARTING INTERVAL')
      GOTO11
3     ITER=1
      IF(FXL.NE.0.)GOTO4
      X2=XL
      FX2=0.
      GOTO8
4     X2=XR
      FX2=0.
      GOTO8
C
C     .....BEGIN REGULA FALSI ITERATIONS .......................R
5     DO7ITER=1,ITMAX
      X2=(XL*FXR-XR*FXL)/(FXR-FXL)
      CALL VAJ(X2,STR)
      FX2=STR
C
C     .....CHECK FOR CONVERGENCE ...............................
      IF(ABS(FX2).LE.EPS)GOTO8
C
C     .....KEEP RIGHT OR LEFT SUBINTERVAL .......................
      IF(FX2*FXL.LT.0.)GOTO6
      XL=X2
      FXL=FX2
      GOTO7
6     XR=X2
      FXR=FX2
7     CONTINUE
      PRINT202,ITMAX
202   FORMAT(1H0,20X,'NO CONVERGENCE AFTER',I3,'ITERATIONS')
8     CF=(2.*((1.-SR+SR*SR)**0.50))
      EH=((2.0-SR)/CF)*X2
      ER=((2.0*SR-1.0)/CF)*X2
      ET=((1.0+SR)/CF)*X2
      FI=(1.-((BETA*((CONS*(1./R1)*X2)+R2))/(EXP((-1.*(1.+SR)*X2
     5)/(2.*((1.-SR+SR*SR)**0.50))))))
      CORR=((FI)**(1./P))
      PRINT31,R1,ITER,X2,EH,ER,ET,FI,CORR,FX2
31    FORMAT(5X,F7.2,I5,4E15.6,3F12.7)
      R1=R1+5.0
      XL=0.01
      XR=0.9
      AZB6(J,1,N)=ET
      AZB6(J,2,N)=ER
20    CONTINUE
      NN(N)=NO
      SWIFT=((4.*P*((1.-SR+SR*SR)**1.5))/(4.-3.*SR-3.*SR*SR+4.*SR*SR
     7*SR))
      PRINT36,SR,SWIFT
36    FORMAT(1H0,15X,'THE SWIFT INSTABILITY STRAIN AT STRESS RATIO(
```

```
      CALL MPLOT(AZ36,KSP,MN,51,101)
1     STOP
      END
C
C================================================================
C     THIS IS FUNCTION SUBROUTINE.
      SUBROUTINE VAJ(X,STR)
      COMMON R1,SR,P,BETA,CONS,R2
      STR=(X-((((4.*R*((1.-SR+SR*SR)**1.5))*((1.-((BETA
     1*((CONS*(1./R1)*X)+R2))/(EXP((-1.+SR)*X)/(2.*((1.-SR+SR*SR)
     2**0.5))))))**(1./P)))/(4.-3.*SR-3.*SR*SR+4.*SR*SR*SR))
1     RETURN
      END
C
      SUBROUTINE MPLOT(A,NASA2,NASA,NLY,NLYX)
C     ************************************************
C
C           A    THIS A 3 DIMENSIONAL MATRIX WHOSE ELEMENTS
C                     ARE AS FOLLOWS:
C     A(I,1,K)=X-CO ORDINATE
C                         A(I,2,K)=Y-CO ORDINATE
C                         I=1,50(NO. OF POINTS)
C                         K=INTEGER WHOSE VALUE DETERMINED
C       BY THE POINT.(TO WHICH GRAPH IT BELONGS
C                                                              TO)
C           NASA2:    NUMBER OF GRAPHS TO BE PLOTTED
C           NASA :    AN ARRAY CONTAINING NUMBER OF POINTS
C                     IN EACH GRAPH.
C           NLY  :    NUMBER OF LINES IN Y-AXIS
C           NLYX :    NUMBER OF LINES IN X-AXIS.
C
C     ************************************************
      DIMENSION X(1000),Y(1000),SX(11),SY(11),ILC(120)
      DIMENSION A(50,2,10),NASA(10),ISYMB(10),IMY(1000)
      DIMENSION ILB(120),ILL(120),XXX(1000),ILD(200)
      DATA ID,IP,IB,IX,IZ/'-','!',' ','*',1H!/
      DATA ISYMB(1),ISYMB(2),ISYMB(3)/'1','2','3'/
      DATA ISYMB(4),ISYMB(5),ISYMB(6),ISYMB(7)/'4','5','6','7'/
      DATA ISYMB(8),ISYMB(9),ISYMB(10)/'8','9','0'/
      NLX=NLYX
      PRINT705
705   FORMAT(1H1)
      N=0
      DO311K=1,NASA2
      DO310J=1,NASA(K)
      N=N+1
      Y(N)=A(J,2,K)
      X(N)=A(J,1,K)
310   IMY(N)=K
311   CONTINUE
      DO 1 I=1,N
      II=1
      DO 2 J=II,N
      IF(Y(I).GT.Y(J))GOTO3
      GOTO2
3     TEMP=Y(I)
      Y(I)=Y(J)
      Y(J)=TEMP
      TEMP=X(I)
      X(I)=X(J)
      X(J)=TEMP
      ITEMP=IMY(I)
      IMY(I)=IMY(J)
      IMY(J)=ITEMP
2     CONTINUE
1     CONTINUE
      XMIN=X(1)
      XMAX=X(1)
      KCHECK=0
      DELY=(Y(1)-Y(N))/(NLY-1)
      DO 4 I=1,N
      IF(X(I).GT.XMIN)GOTO6
      XMIN=X(I)
6     IF(X(I).LT.XMAX)GOTO4
      XMAX=X(I)
4     CONTINUE
      DELX=(XMAX-XMIN)/(NLX-1)
      PRINT93,DELY,DELX
93    FORMAT(35X,'DELY=',E15.8,10X,'DELX=',E15.8/)
      JX=NLX/10+1
      JY=NLY/5+1
      DO 5 I=1,JY
```

```
      DO 7 I=2,NLX
      II=I-(I/10)*10
      IF(II.NE.1)GOTO 9
      TLC(I)=ID

      GOTO7
9     TLD(I)=ID
7     CONTINUE
      TLC(1)=ID
      TLC(NLX)=ID
      TLB(1)=ID
      TLB(NLX)=ID
      TLD(1)=ID
      TLD(1)=ID
      TLD(NLX)=ID
      PRINT 92,(SX(I),I=1,JX)
      PRINT 91,(TLC(I),I=1,NLX)
92    FORMAT(15X,11(F9.3,1X))
91    FORMAT(20X,102A1)
401   FORMAT('   8450')
      IF(XMIN*XMAX.GE.0)GOTO16
      NZZ=-XMIN/DELX
      KCHECK=1
16    NI=0
      Y(N+1)=Y(N)-DELY
      DO10I=1,N
      MX=(Y(I)-XMIN)/DELY+1
      MY=(Y(1)-Y(I))/DELY+0.5
      MY1=(Y(1)-Y(I+1))/DELY+0.5
      NK=MY1-MY
      IF(NK-1)61,62,63
61    TLC(MX)=ISYMB(IMY(I))
      GOTO10
63    NK=NK-1
      TLC(MX)=ISYMB(IMY(I))
      NP1=MY-(MY/5)*5
      NP2=MY/5+1
      IF(KCHECK.NE.1)GOTO300
      TLC(NZZ)=IZ
300   IF(NP1.NE.0)GOTO303
      IF(MY.EQ.NLY .OR.MY.EQ.0)GOTO302
      DO 301 JBI=1,NLX
      IF(TLC(JBI).NE.IB)GOTO301
      TLC(JBI)=ID
301   CONTINUE
302   PRINT 96,SY(NP2),(TLC(KX),KX=1,NLX)
      GOTO304
303   PRINT 97,(TLC(KL),KL=1,NLX)
C     ****************************************
304   DO 65 KP=1,NK
      NP1=(MY+KP-1)/5.+1
      NP=MY+KP-(NP1-1)*5
      IF(NP.NE.0)GOTO71
      IF(KCHECK.NE.1)GOTO307
      TLD(NZZ)=IZ
307   PRINT96,SY(NP1),(TLD(KL),KL=1,NLX)
      GOTO65
71    PRINT97,(TLB(KL),KL=1,NLX)
65    CONTINUE
97    FORMAT(20X,102A1)
      GOTO195
C     ****************************************
62    CONTINUE
      TLC(MX)=ISYMB(IMY(I))
      NP1=MY-(MY/5)*5
      NP2=MY/5+1
      IF(KCHECK.NE.1)GOTO78
      TLC(NZZ)=IZ
78    IF(NP1.NE.0)GOTO73
      IF(MY.EQ.NLY-1 .OR.MY.EQ.0)GOTO83
      DO 74 JBI=1,NLX
      IF(TLC(JBI).NE.IB)GOTO74
      TLC(JBI)=ID
74    CONTINUE
83    PRINT 96,SY(NP2),(TLC(KX),KX=1,NLX)
      GOTO195
73    PRINT 97,(TLC(KL),KL=1,NLX)
96    FORMAT(5X,E15.8,102A1)
C     ****************************************
195   CONTINUE
      DO66KO=1,NLX
```